



Article

Efficient Removal of Tannic Acid from Olive Mill Wastewater Using Carbon Steel Slag

Otmane Sarti ¹, Fouad El Mansouri ^{2,*}, El Habib Yahia ¹, Emilia Otal ³, José Morillo ³ and Mohamed Saidi ¹

¹ Laboratory of LAMSE, Faculty of Sciences and Techniques of Tangier, P.O. Box 416, Tangier 90000, Morocco

² Research Team: Materials, Environment and Sustainable Development (MEDD), Faculty of Sciences and Techniques of Tangier, Abdelmalek Essaâdi University, P.O. Box 416, Tangier 93000, Morocco

³ Department of Chemical and Environmental Engineering, University of Seville, Camino de Los Descubrimientos, s/n, 41092 Seville, Spain

* Correspondence: fouad.elmansouri@etu.uae.ac.ma; Tel.: +212-662-102-847

Abstract: Mediterranean countries experience a large production of olive oil, thus generating huge quantities of non-biodegradable vegetation waters. The discharge of these effluents into aquatic environments seriously affects the quality of surface waters. This study investigated the potential use of carbon steel slag (SS) as an adsorbent and improver for reducing olive mill wastewater (OMWW) toxicity. The elemental and structural characterization of SS was carried out using inductively coupled plasma-optical emission spectrometry (ICP/EOS), X-ray fluorescence (XRF), X-ray powder diffraction (XRD), scanning electron microscopy (SEM), and Brunauer–Emmett–Teller (BET) analysis. OMWW characterization indicated that the effluent was acidic in nature, with a pH of 4.8, a higher conductivity reaching 14.92 mS/cm, higher COD of 157.31 g/L, rich in organic matter 112.33 g/L, and total phenolic compounds of 11.13 g/L. The neutralization capacity of SS was demonstrated by reducing the OMWW's acidic character. Afterward, the adsorption of tannic acid (TA) was investigated using SS. Parameters such as contact time, initial TA concentration, adsorbent dosage, pH, and temperature were investigated. The kinetic study indicated that the adsorption of TA onto SS fitted well with the second pseudo-order ($r = 0.99$) and Elovich ($r = 0.98$) models, indicating that the adsorption of TA was mainly chemical and depends on the reactions of oxide hydrolysis and hydroxides dissolution. Moreover, Langmuir isotherm has greatly described the adsorption of TA on SS ($R = 0.997$), suggesting that the surface of SS is homogenous, and the adsorption occurs mainly in monolayer. The maximum adsorption capacity reached 714.28 mg/g, indicating the higher capacity of SS to reduce the polyphenolic compounds in OMWW. This study demonstrated that SS residue from the steelmaking industry could present a highly interesting material for OMWW remediation.

Keywords: OMWW; adsorption; carbon steel slag; tannic acid



Citation: Sarti, O.; El Mansouri, F.; Yahia, E.H.; Otal, E.; Morillo, J.; Saidi, M. Efficient Removal of Tannic Acid from Olive Mill Wastewater Using Carbon Steel Slag. *C* **2023**, *9*, 32. <https://doi.org/10.3390/c9010032>

Academic Editors: Indra Pulidindi, Pankaj Sharma and Aharon Gedanken

Received: 8 February 2023

Revised: 4 March 2023

Accepted: 8 March 2023

Published: 12 March 2023



Copyright: © 2023 by the authors. Licensee MDPI, Basel, Switzerland. This article is an open access article distributed under the terms and conditions of the Creative Commons Attribution (CC BY) license (<https://creativecommons.org/licenses/by/4.0/>).

1. Introduction

In the Mediterranean region, olive oil (*Olea europaea* L.) is increasingly consumed for its bioactive content, organoleptic properties, medicinal value, and protection against certain diseases [1–3]. In addition, the Mediterranean countries are responsible for 98% of olive oil production worldwide [4]. However, regardless of its economic importance, the extraction of olive oil is associated with some environmental impacts, such as water pollution, soil deterioration, and air emissions [5]. Olive oil extraction generates solid wastes composed of wet pomace formed from the pulp and pits of olives and a liquid effluent called olive mill wastewater (OMWW) or sometimes vegetable waters. Generally, the solid by-product does not constitute disposal problems as long as specific industrial oil mills use it to produce a so-called pomace oil by (chemical) solvent extraction. After the extraction, the pomace serves as fuel in industrial boilers, ovens, and public baths. In contrast, the liquid effluent is rarely treated and dumped directly into natural waters. OMWW is composed mainly of

vegetation water from olive, process water (washing and treatment), a portion of the pulp, and residual oil [6]. The olive oil extraction generates quantities of OMWWs ranging from 0.3 to 1.1 m³ per ton of olives processed, depending on the olive oil extraction technique [7–9]. This liquid effluent is characterized by a cloudy appearance, a strong odor of olive oil, an intense brown-red to black color, and is heavily loaded with organic matter and suspended solids [10]. Eroğlu et al. [11] reported that the black-brownish color characteristic of this effluent is due to the low biodegradability of phenolic compounds.

Recently, great efforts have been made to reduce the toxicity of OMWWs, and various authors discussed the possibility of OMWW treatment through physical, chemical, and biological processes. Among these methods, combined coagulation–flocculation with hydrogen peroxide oxidation [12], biological treatments [13], photocatalysis [14], solvent extraction followed by photo-Fenton oxidation [15], electrocoagulation [16], aerobic biological treatments [17], and anaerobic digestion treatment [18] were investigated. The removal of phenolic compounds from OMWWs has recently gained more attention. Among the existing methods, adsorption is regarded as the most appropriate treatment for removing polyphenols since it is a cost-effective operation that can be handled without needing higher temperatures, specific methodology, or large energy input [19,20].

Oil mill waste contains a high concentration of phenolic compounds such as polyphenols, including condensed and hydrolysable tannins, which require proper disposal to avoid environmental hazard [21]. Besides the olive mills wastewater, tannic acid may also be found in effluent from the coir and cork processing industries, as well as the plant medicine, paper, and leather industries [22,23]. Tannic acid (TA) is a natural organic matter (NOM) component present in surface and groundwater generated from the degradation of biomass [23,24]. Because it can generate carcinogenic disinfection by-products (DBPs) during the chlorination process, TA might contaminate drinking water [23,24]. Since it is a water-soluble polyphenolic molecule, TA is also hazardous to aquatic organisms such as algae, phytoplankton, fish, and invertebrates [23]. Consequently, eliminating TA from water and wastewater is critical for both human health and the ecosystem [23]. Several attempts were made to remove TA from aqueous solution, e.g., polyaniline (PANI) prepared by chemical oxidation [25], electrochemical processes [26], coagulation-adsorption [27], membranes ultrafiltration [28], and biological processes [29]. Among these methods, adsorption has been widely used to remove TA from water and wastewater using different adsorbents such as carbon nanotubes [30], amino-functionalized magnetic mesoporous silica [23], silk fiber [31], polystyrene microplastics [32], attapulgite/CoFe₂O₄ [33], chitosan-montmorillonite composites [34], chitosan and activated clay [35], and functionalized zeolites [36].

Steel slag (SS) is a solid by-product of the steel-making industry generated in huge quantities (thousands of tons) in different regions of the world. The production of 1 ton of steel is associated with the production of 0.13–0.2 tons of slags [37,38]. The steel slag (SS) is an alkaline residue representing a higher surface area and porosity and mainly consisting of oxides (CaO, MgO, SiO₂, Al₂O₃, and Fe₂O₃). Investigations on the use of steel slag in water treatment have been carried out to achieve effective and comprehensive reuse of this solid waste, thereby presenting a low-cost solution for wastewater treatment [39]. Some researchers have already demonstrated satisfactory results when applying SS as an adsorbent to remove ammonia, phosphate, hydrogen sulfide, cadmium Cd (II), and arsenic As (V) [40–44]. Furthermore, due to the greater amount of metal oxides such as CaO and MgO, the SS residues displayed effectiveness in terms of CO₂ capture [45–48].

This research presents a new low-cost and simple approach for treating olive mill wastewaters (OMWWs) utilizing steel slag (SS) waste from industrial steelmaking. The physicochemical properties of OMWW were analyzed. Afterward, various techniques were employed to characterize the steel slag used in this work (ICP/OES, XRF, XRD, SEM, and BET). Before Bach experiments, OMWW was treated with different ratios of raw SS to investigate the direct effect of SS addition on the OMWWs' pH neutralization. The adsorption behavior of tannic Acid (TA) under different conditions (contact time, initial

TA concentration, adsorbent mass, pH, and temperature) was investigated. Adsorption isotherms, kinetics, and adsorption mechanisms were discussed. The contribution of this study is expected to reduce the acute acidity of vegetation waters and the high polyphenolic content of OMWWs.

2. Materials and Methods

2.1. Olive Mill Waste Water (OMWW)

The olive mill effluent investigated in this study derived from a traditional oil-producing plant located in Chefchaouen city in the Northwest of Morocco. Sampling was carried out in an oil mill during the pressing phase of oil production. The newly collected olive mill wastewater was transported to the laboratory in polyethylene bottles (5 L), carefully filled, and tightly sealed to maintain an oxygen-free environment. To avoid fermentation, OMWW samples were stored in the dark at 4 °C in a non-oxygenated environment.

2.2. Olive Mill Wastewater Characterization

The pH and Electrical conductivity (EC) measurements were made for a sample of undiluted raw olive vegetable water using a pH and EC meter brand HANNA HI2550 (Hanna Instruments, Woonsocket, RI, USA). After calibrating the pH meter, the measuring electrode was immersed in a flask containing 50 mL of effluent. The OMWW water content was determined by the difference between the fresh weight of the effluent sample and its dry weight (after drying in an oven at 105 °C for 24 h) and expressed as a percentage of humidity, while the solid residue was considered as dry matter (DM) expressed in (g/L). The organic matter (OM) was determined by the loss on ignition (LOI) method at 525 °C for 2 h and expressed as g/L. The COD was determined using JP SELECTA BLOC DIGEST apparatus (JP Selecta, Barcelona, Spain). The oxidation was carried out by the potassium dichromate method. This method is based on boiling oxidation (150 °C for 2 h) of reducing materials with an excess of ($K_2Cr_2O_7$) in an acidic medium (H_2SO_4), and in the presence of silver sulfate as a catalyst and sulfate mercury as a chloride complexing agent. The COD is evaluated at the end of the reaction by taking a suitably diluted sample before oxidation 100 times. This measurement was made for raw OMWW samples according to the NFT 90–101 standardized method. Determining the biological oxygen demand (BOD) is an essential parameter for treating liquid effluents such as OMWWs. The 5-day biochemical oxygen demand BOD₅ was determined by a respirometry method using an OxiTop system (WTW, Xylem, Weilheim, Germany). The total phenolic content was determined following the Folin–Ciocaltau method [49] using tannic acid (tannic acid powder, puriss; Sigma Aldrich, St. Louis, MO, USA) as a standard and equivalent of the total polyphenolic concentration contained in OMWW. The concentration of tannic acid was quantitatively determined at 760 nm using the JASCO 630 Double Beam UV/Visible spectrophotometer (JASCO, Tokyo, Japan).

2.3. Steel Slag (SS) Characterization

The steel manufacturing process in electric arc furnaces consists of two stages: the first, called primary metallurgy or fusion, in which raw materials are fused in an electric arc furnace (EAF), and the second, called secondary metallurgy or molten bath refining, which begins in the electric furnace and ends in the ladle furnace. The steel slag used in this study was produced in Sevilla, Spain. The plant produces two types of SS. Black slags generated during the fusion step are very hard materials, unlike the white slags produced during the refining phase, which is a relatively soft and finer material and has high basicity due to the percentage of free lime. The white steel slag used in this study was collected from the ladle furnace. The material was characterized by a crumbly structure and a softer texture, the sample was sieved using a 200-micron mesh, and no modification was performed on the raw SS (Figure 1). The pH of the SS sample was measured following the 9045D method using a pH meter (Thermo Fisher Scientific, Waltham, MA, USA). The determination of major elements and trace elements in the SS was

carried out using inductively coupled plasma–optical emission spectroscopy (ICP/OES, Agilent 5100, Tokyo, Japan) after acid digestion ($\text{HNO}_3\text{-HCL}$ 1:3 (*v/v*)) using a DigiPREP heating and digestion blocks (SCP Science, Montreal, QC, Canada). The Brunauer–Emmett–Teller (BET) analysis was employed to investigate the pore size distribution, specific surface area, and nitrogen adsorption–desorption curve of SS. The analysis was performed using BET Surface Area Analyzer Micromeritics Tristar II 3020 (Micromeritics Instr. Corps., Norcross, GA, USA). The structural and morphological surface of the steel slag sample was determined using scanning electron microscopy (SEM) (SEM, Hitachi, Tokyo, Japan, S-4800). Simultaneously, the elemental composition of the SS was determined using an X-ray fluorescence spectrometer (XRF, PANalytical Axios FAST simultaneous WDXRF, Malvern PANalytical Ltd., Almelo, The Netherlands). The crystalline composition of SS was analyzed by X-ray diffraction (XRD) using a PANalytical X'Pert Pro X-ray diffractometer (Malvern PANalytical Ltd., Almelo, The Netherlands). All the experiments were carried out using ultrapure Mllii-Q water.



Figure 1. Olive mill wastewater (OMWW) and steel slag (SS) samples.

2.4. Effect of SS Addition on Raw OMWW

In order to investigate the effect of SS addition on the OMWW pH variation, The OMWW was treated with different ratios of SS. Different doses of SS (0.5-1-2-3-4-5-10-20-30-40 g/L of OMWW) were dispersed in the raw OMWW samples and stirred. Afterward, the pH variation of OMWW was measured at different contact times (30-60-90-120-150-180 min) and after 24 h.

2.5. Adsorption Study

For the adsorption study, the influence of different parameters on the TA-SS adsorption mechanism, namely the time of equilibration, the pH, the initial concentration of the solute, and the influence of the temperature, were investigated.

The batch experiments were performed to assess the TA adsorption isotherms onto SS. Accordingly, 100 mg of steel slag SS was added to a 150 mL flask containing 100 mL of TA solution with initial concentrations ranging from 50 to 1000 mg/L and a pH of 6 (pH solution). The flasks were placed inside an incubator and stirred at 25 °C for 24 h. After achieving adsorption equilibrium, the adsorbent particles were centrifuged from the aqueous solution, filtered, and the residual TA concentrations in the aliquot were evaluated using a UV-vis spectrometer with a detection wavelength of 760 nm. The equilibrium of TA adsorption capacity was calculated using Equation (1):

$$q_e = \frac{(C_0 - C_e)V}{M} \quad (1)$$

Noting that q_e is the adsorbed amount of tannic acid in mg/g, V the volume of solution in mL, C_e concentration at the equilibrium in mg/L, and C_0 initial concentration of TA in mg/L, and M is the SS mass in (g).

In order to study the time effect, the experiments were carried out by varying the contact time from 30 to 240 min. The pH solution, temperature, and SS mass were kept constant. The studied pH values range from 2 to 11 (the acidic and basic pH values obtained by adjusting the initial pH of the adsorbate solutions using NaOH and HCl solutions). The suspensions were stirred to the equilibrium time determined by the kinetic study of adsorption. The other parameters were held constant. The optimal temperature of adsorption was carried out by Bach experiments at 15, 30, 45, and 60 °C. The remaining parameters were kept constant. Adsorption kinetics were investigated using the pseudo-first-order, pseudo-second-order, Elovich, and intraparticle diffusion models. The modeling of isotherms was performed by plotting the linear form of Langmuir and Freundlich isotherms.

3. Results and Discussion

3.1. The Results of OMWW Characterization

The OMWWs are generally characterized by an acid pH of 3–6, rich in organic matter, and low in biodegradable polyphenols (0.5–24 g/L) [19,50–53]. In addition, these effluents displayed higher electrical conductivity (EC), chemical oxygen demand (COD), and biological oxygen demand (BOD) ranging from 40–220 g/L and 35–110 g/L, respectively [54,55]. The pH of the sampled OMWW was 4.8. As a result, the nature of this effluent is acidic. The existence of organic acids (phenolic acids, fatty acids, etc.) capable of releasing positively charged protons H^+ is primarily responsible for this acidity. Table 1 represents the main results of OMWW characterization. The measured electrical conductivity (EC) of OMWW was 14.92 mS/cm, resulting mainly from the higher concentration of dissolved minerals and salts. Olives acquire a significant amount of water during the pressing process. The OMWW contained 83.04% water content and a relative dry matter (DM) of 177.04 g/L. Total suspended matter (TSM) concentration was high in OMWW, showing a value of 98.85 g/L, these solid materials are essentially organic in nature and generate increased turbidity in the receiving environment. The OM loading in the OMWW sample was higher, reaching 112.33 g/L. Furthermore, the COD and BOD₅ of OMWW were 157.31 and 35.40 g/L, respectively, indicating severe organic pollution of this effluent and its limited eputation capability. Similarly, OMWW had a higher polyphenolic concentration of 11.13 g/L, indicating an abundance of non-biodegradable phytotoxic compounds. According to Bouknana et al. and El Gnaoui et al. the poor biodegradability of OMWW is mainly related to their high polyphenol and COD concentrations, limiting thus any biological decomposition [56,57].

Table 1. Physicochemical characterization of OMWW.

Parameter	Unit	Value
pH	–	4.80
EC	ms/S	14.92
Water content	%	83.04
Dry matter (DM)	g/L	177.04
Total Suspended matter (TSM)	g/L	98.85
Organic Matter (OM)	g/L	112.33
DOC	g/L	157.31
BOD ₅	g/L	35.40
Total phenols (as tannic acid)	g/L	11.13

3.2. Steel Slag (SS) Characterization

3.2.1. Physicochemical Characterization

The main physicochemical characterization results are shown in Table 2. The white slag sampled from the ladle furnace has a higher alkalinity with a pH of 12.58; This higher value is due to the dissociation of calcium and magnesium hydroxides, which allows the formation of OH[−] ions, and thus a more elevated alkalinity. Indeed, the calcium content was higher and represented 15.05% of the total SS residue. This higher calcium content in SS is attributable to the introduction of CaO (free lime) and dolomite as fluxing agents to remove impurities from the molten steel contained in the Ladle furnace [58]. Evaluating SS toxicity is a necessary step to ensure the safe utilization of SS residue and avoid the environmental hazard. The SS leaching experiments are conducted to gather more information about the possible release of contaminants from the slag samples into the nearby environment as a result of weathering mechanism. Additionally, trace elements concentrations in SS leachates could be compared to water and soil quality standards to determine the possibly harmful effects. There are generally two methodologies regarding trace elements leaching from solid wastes. The first being the total concentration test of trace elements which is intended to estimate the total trace elements content through heating and aggressive acid digestion following (U.S. EPA. “Method 3050B”), methodology followed during this study. While a second methodology based on (EPA method 1311-Toxicology Characteristic Leaching Test) is designed to determine the mobility of trace element in the liquid phase. As a result, the SS toxicity depends on their leaching capacity, and not directly on the totally available trace elements. In this study, the total concentration of trace elements in SS has decreased in the following sequence Zn > Cu > Cr > Pb > Ni > As > Mo > Cd > Co > Hg. Among the analyzed trace elements, only Zinc concentration exceeded 390 mg/Kg. According to De Martino et al. [59] Zinc-Aluminum hydroxide could decontaminate OMWW by reducing the phenolic compounds up to 90%. The concentrations of Cu, Cr, Pb, and Ni displayed natural background levels and did not exceed the permissible level for waste disposal. At the same time, trace elements such as As, Cd, Co, and Hg were relatively low in the SS. A study of SS toxicity of heavy metals showed a relatively higher total concentrations than the present study, e.g., Cd = 89.65; As= 23.13; Cu = 70.38; and Pb = 978.41 mg/Kg [60]. However, according to this study, the Toxicology Characteristic Leaching Test (method 1315) displayed limited mobility of heavy metals indicating a secure disposal condition. In addition, the SS used in this study is intended to remediate a highly loaded organic wastewater and not directly discharged into the environment. Generally, the white SS from the Ladle furnace is usually less toxic because most trace elements are accumulated in the black slags produced during the fusion process. Furthermore, due to the limited solubility of its mineral phases, Ladle furnace slag has negligible environmental consequences [61]. The trace elements analysis of SS generally demonstrated low concentrations with a total

weight of less than 0.1% in volume. These results confirm that white SS from the refining phase of the steelmaking industry could be used for OMWWs treatment.

Table 2. Physicochemical characterization of SS.

Parameter	Unit	Value
pH	–	12.58
Ca	%	15.05
As	mg/kg	8.86
Cd	mg/kg	0.91
Co	mg/kg	0.53
Cu	mg/kg	71.23
Hg	mg/kg	ND
Mo	mg/kg	4.65
Ni	mg/kg	23.19
Pb	mg/kg	24.56
Zn	mg/kg	390.86
Cr (total)	mg/kg	44.58

3.2.2. Elemental Composition by XRF

Table 3 shows the elemental composition of SS. CaO, MgO, SiO₂, and Al₂O₃ were the main oxides present in SS, representing a percentage higher than 80%, with a predominance of Ca followed by Mg oxides. Other oxides such as FeO, MnO, NaO, K₂O, TiO, P₂O₅, and SO₃ were present in a lower percentage of 3.55%. In contact with water, oxides such as CaO, MgO, and other alkaline metals dissociate and form hydroxide groups. The mixed hydrolysis of these hydroxides liberates hydroxyl (OH[−]) groups and cationic metals such as Ca²⁺ and Mg²⁺ in water [39]. The free (OH[−]) contained in an aqueous solution could be responsible for the adsorption, ion exchange, and precipitation processes of contaminants in wastewater [39].

Table 3. Chemical composition of steel slag by XRF spectrometry.

Element	SiO ₂	Al ₂ O ₃	Fe ₂ O ₃	MnO	MgO	CaO	Na ₂ O	K ₂ O	TiO ₂	P ₂ O ₅	SO ₃	L.O.I
SS	11.64	5.92	1.09	0.64	22.6	40.2	0.26	0.06	0.27	0.03	1.2	15.11

3.2.3. XRD Characterization of Steel Slag

The XRD patterns show the main identified crystalline phases contained in the raw SS (Figure 2). The profile displays a heterogeneous composition with various mineralogical phases composed mainly of oxides and hydroxides. The following mineralogical phases were the major identified patterns in the SS sample: (1) katoite Ca₃Al₁₂(SiO₄)(OH)₈; (2) Magnesium hydroxide base (Mg(OH)₂); (3) Calcium Silicate (Ca₂SiO₄), (4) portlandite (Ca(OH)₂); and (5) calcium silicate hydrate (3 CaO, 2SiO₂, 3H₂O). These results confirm that the dominant oxides CaO, MgO, SiO₂, and Al₂O₃ previously determined by XRF were the main constituent of SS mineralogical phases, demonstrating heterogeneity in the distribution of SS oxyhydroxides. The obtained XRD pattern phases were much similar to those provided by Navarro et al. [62]. Furthermore, Rađenović et al. [61] stated that silicate calcium was the main constituent of Ladle furnace slags under its different mineralogical forms. The same authors have reported that the presence of CaO, MgO, and SiO₂, in addition to aluminum silicates, confers to SS the adsorption properties.

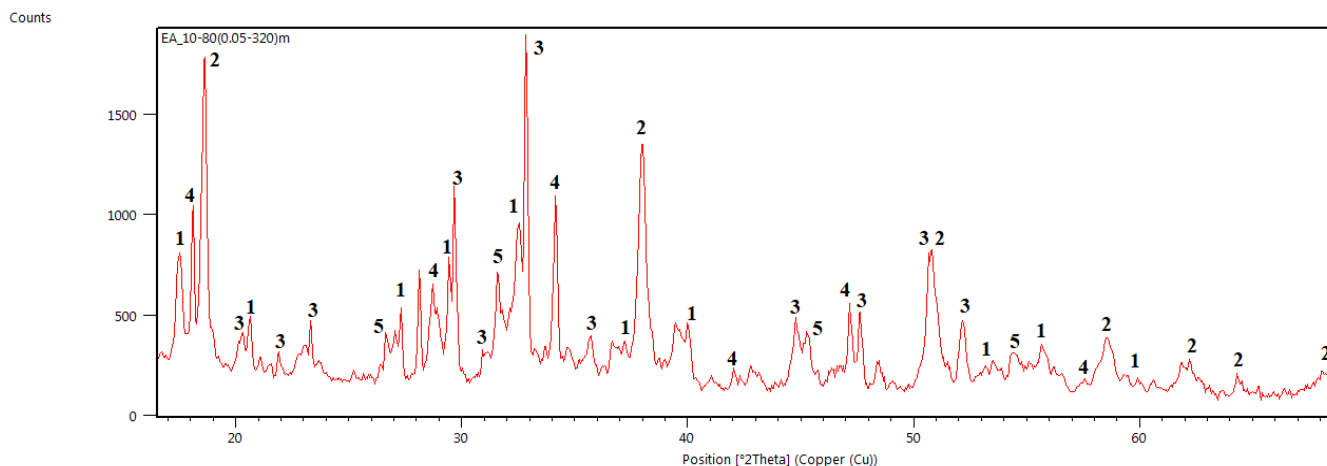


Figure 2. Main identified phases detected in steel slag sample: (1) Calcium Aluminum Silicate Hydroxide; (2) Magnesium Hydroxide; (3) Calcium Silicate; (4) Calcium Hydroxide; (5) Calcium Silicate Hydroxide Hydrate.

3.2.4. BET Characterization of the Steel Slag Adsorbent

Table 4 represents the characteristics of the SS surface by the BET method. The studied steel slag was characterized by a surface area of 10.90 m²/g, representing a great surface area compared with other SS studies. Furthermore, the SS demonstrated a larger Langmuir surface area and pore diameter distribution of 15.61 m²/g and 12.55 nm, respectively. The total pore volume was 0.035 cm³/g. It is also noted that the micropore surface area was low in SS, representing only 0.86 (m²/g). Wang et al. [23] studied the adsorption of TA on amino-functional magnetic mesoporous silica. They reported that efficient and rapid adsorption of TA is achieved due to the mesoporous nature of the adsorbent. The N₂ adsorption–desorption curve shows that SS’s maximum N₂ adsorption capacity reached 31.16 (cm³/g STP) (Figure 3). The SS adsorption–desorption isotherm belongs to type IV, which is characteristic of mesoporous material. Effectively, the pore size distribution confirms that steel slag contains meso- and macropores structure mainly distributed between 10 and 100 nm.

Table 4. Steel slag (SS) BET surface area characteristics.

Sample	BET Surface Area (m ² /g)	Langmuir Surface Area (m ² /g)	Micropore Area (m ² /g)	Total Pore Volume (cm ³ /g)	Pore Diameter (nm)
SS	10.90	15.61	0.86	0.035	12.55

3.2.5. Morphological Characterization of Steel Slag by SEM

The SEM micrographs of SS are shown in Figure 4. Firstly, the particle size distribution shows that SS exclusively has a low grain size distribution of <5 μm according to the SEM scale. While some minerals, probably Quartz (SiO₂) represent a relatively higher diameter. The morphology of SS was quite heterogeneous, displaying a rich mineralogical surface. In addition, SEM micrographs show pores of various sizes distributed over the surface of SS and oxides, confirming that the SS contains macro and mesopores as reported by BET analysis. These pores were predominantly large in diameter and volume, with low microporosity observed. Furthermore, it was clear that the surface of SS was quite rich in oxides, which display heterogeneous shapes and forms.

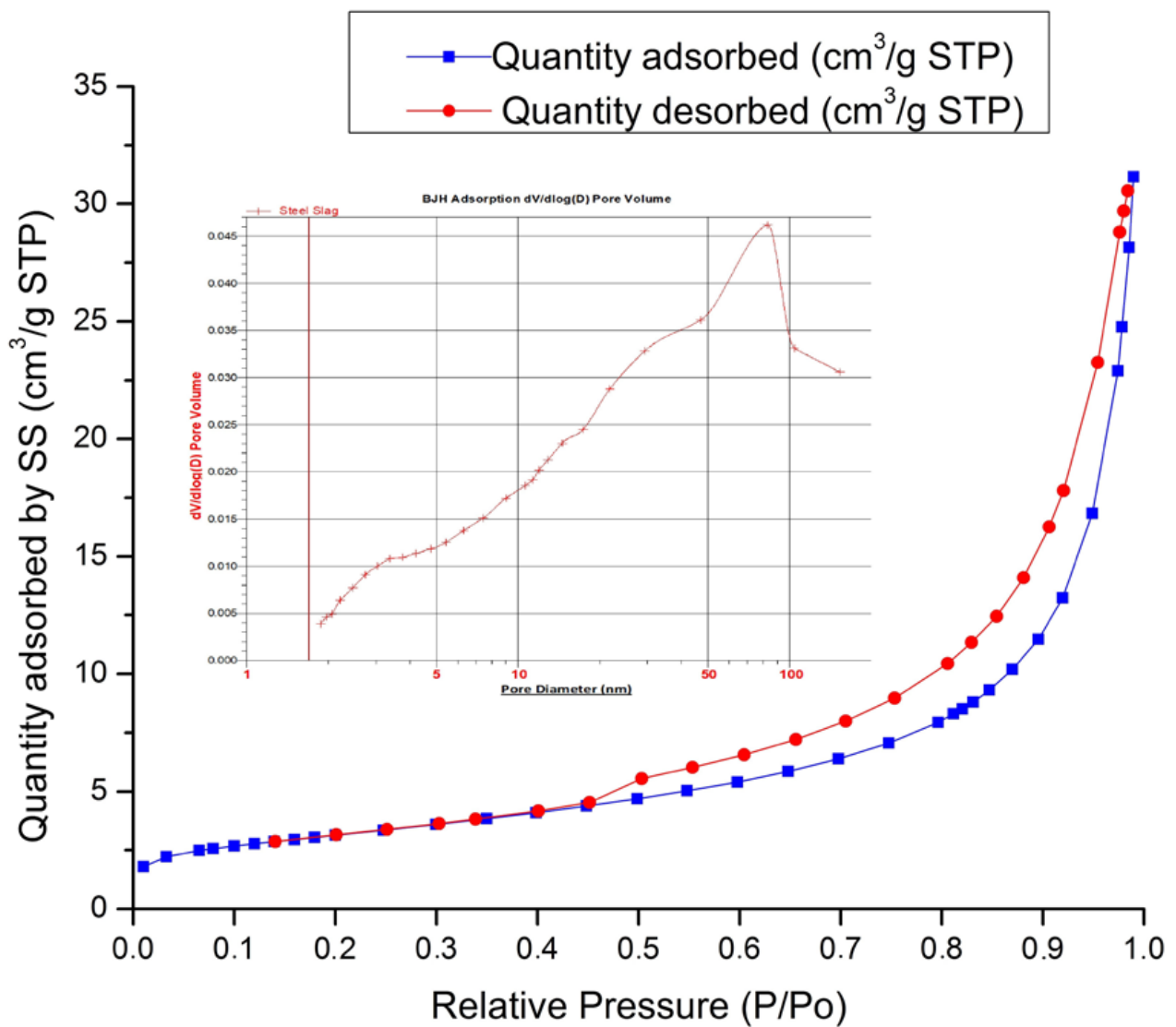


Figure 3. N₂ adsorption-desorption curve and pore diameter distribution of steel slag.

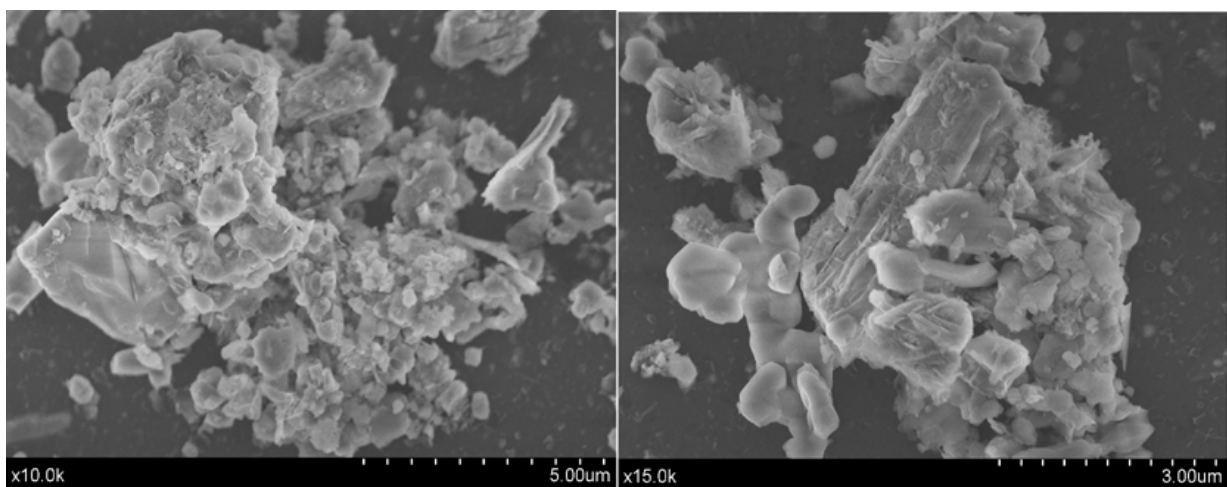


Figure 4. SEM micrographs of steel slag adsorbent at different magnitudes.

3.3. Study of OMWW Neutralization by Steel Slag (SS)

Olive mill wastewater's acidity is one of the most preoccupations that affect the quality of natural waters. This acidity is mainly due to the organic acids and polyphenols-rich wastewater.

Depending on disposal specifications, this experiment could determine the amount of SS needed to raise the OMWW to a given pH. For this reason, OMWW was treated with different dosages of SS. The variation of OMWW pH as a function of SS dosage is highlighted in Figure 5. It was obvious that the pH of OMWW increases parallelly with increasing time and SS mass. By considering neutral condition (pH = 7) as the appropriate pH value for OMWW disposal/treatment. The addition of 0.5, 1, 2, 4, 6, and 8 g_(SS)/L_(OMWW) increased the pH of OMWW gradually from 4.8 to 6.54 after 24 h of agitation. While a neutral pH of 7.18 was achieved only after 24 h of agitation by adding 10 g_(SS)/L_(OMWW) as the minimum required dose. For the remaining doses, 20 g/L and 40 g/L, neutral pH of 7.33 and 7.3 was reached rapidly after 120 and 60 min, respectively. It is to note that the maximum recorded pH was 9.02 after 24 h of agitation and 40 g_(SS)/L_(OMWW). The process of pH augmentation in OMWW could be explained by the dissociation of (Ca(OH)₂) and (Mg(OH)₂) hydroxides resulting from the hydrolysis of metal oxides such as CaO, MgO, and Al₂O₃. This dissociation results in the release of free cations and hydroxyl groups (OH⁻) in the solution, which raises the pH by neutralizing the OMWW's organic acids. According to XRD and XRF characterization results, the studied SS was composed mainly of Hydrated lime (Ca(OH)₂), dolomitic lime (Mg(OH)₂), free lime CaO, and other alkaline metals. Lime is widely reported for its efficiency in OMWW treatment [63–66], e.g., Aktas et al. found that applying 40 g/L of lime for OMWW treatment raised the pH to 12 and removed 73% and 40% of polyphenols and COD, respectively [67]. Accordingly, SS could be considered a liming agent given its high content of dolomite (CaMg(CO₃)₂) and portlandite (Ca(OH)₂). Similarly, Sarti et al. demonstrated the potential use of olive pomace biomass slag, which contains a similar composition as SS, to neutralize acidic agricultural sandy soils [68]. Therefore, regardless of the potential unexplored effects of OMWW treatment by SS. It could be deduced that the application of SS could at least neutralize OMWW and probably reduce COD and other polyphenolic compounds.

3.4. Adsorption of Tannic Acid (TA) on Steel Slag (SS)

3.4.1. Adsorption Kinetics

The kinetic of TA adsorption on SS is highlighted in Figure 6. Results show that TA is adsorbed on the SS matrix with the same kinetics for the three initial concentrations; a maximum adsorption of TA was noticed (0–45 min), during which more than 92, 80, and 75% of the adsorption capacity was reached for an initial TA concentration of 100, 200, and 300 mg/L, respectively. While a relatively slow to constant adsorption was observed between 45 and 225 min, after 24 h (1440 min), no effective change was highlighted in the adsorption rate allowing us to define 225 min as the optimum equilibrium time since more than 90% of TA removal is achieved during this contact time. These results suggest that the adsorption equilibrium of TA depends either on the initial concentration of TA or the equilibrium time. Tannic acid is a weak acid, and therefore its reaction with a strong base such Ca(OH)₂ and/or Mg(OH)₂ could be responsible for the formation of insoluble precipitates. In this study, the primary preproposal process of TA adsorption on SS was regarded as chemical because of the rich accessibility of oxides and hydroxides on the SS surface. Therefore, the following reactions are considered in the process of adsorption.



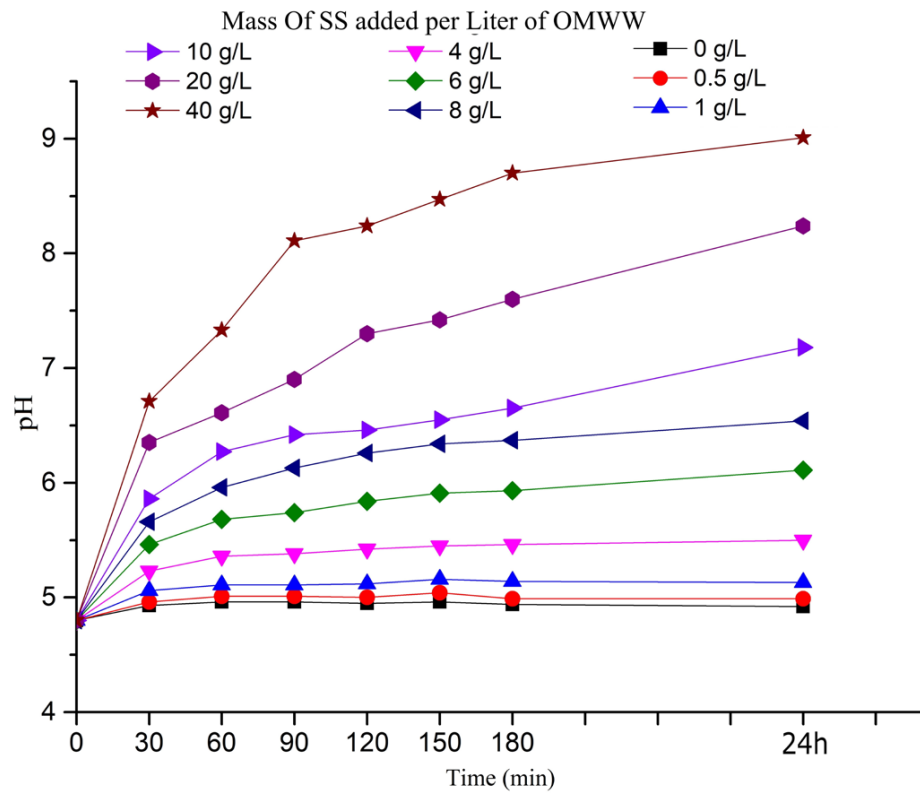


Figure 5. pH variation of OMWW as a function of time and steel slag dosage.

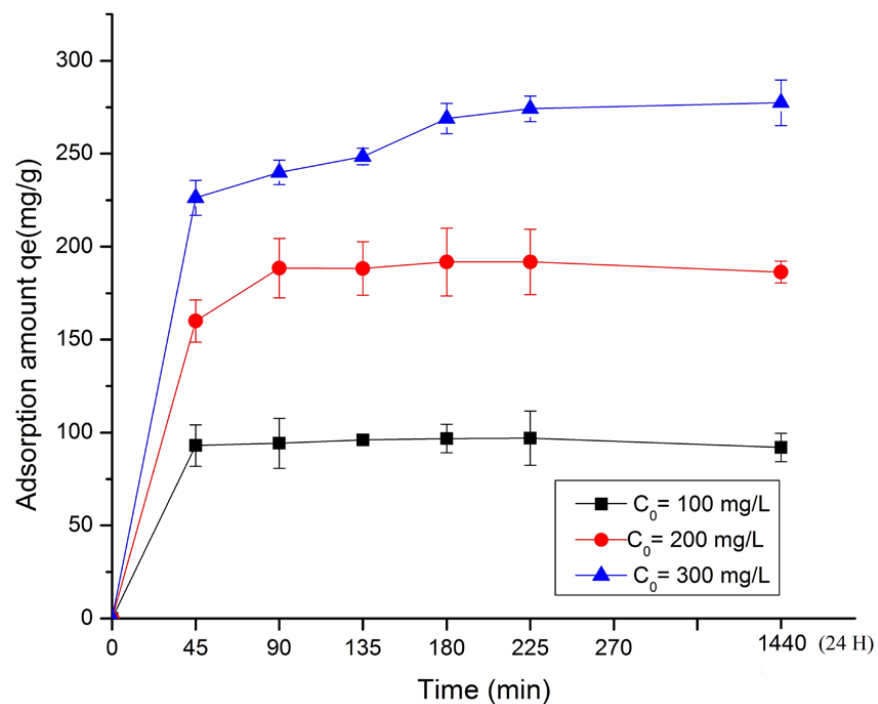
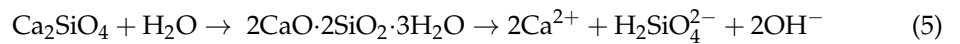
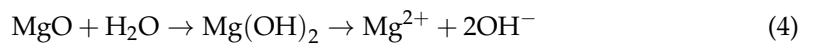


Figure 6. Effect of time on the adsorption of TA by SS ($m = 100$ mg; $V = 100$ mL; concentration = 100, 200 and 300 mg/L; $\text{pH} = 5.8 \pm 0.1$; $T = 293 \pm 1$ K; Agitation = 500 rpm).

Murdiati et al. reported that the reaction between TA and $\text{Ca}(\text{OH})_2$ generates binded insoluble complexes [69]. Other authors added that complexation through chelation is possible between calcium and TA [70]. In comparison, other authors confirmed that the presence of Ca^{2+} in the solution greatly enhanced the adsorption of TA on polystyrene microplastics. In another study, Murdiati et al. studied the capacity of polyvinylpyrrolidone (PVP), $\text{Ca}(\text{OH})_2$, and activated charcoal to precipitate TA in solution and found that $\text{Ca}(\text{OH})_2$ was more effective in the precipitation process of tannin and tannic acid [71]. This explains the fast adsorption of low TA concentration by SS, and may suggest that the formation of SS-TA complex depends on the initial TA concentration and the accessible free cations and hydroxyl groups in the solution. However, the adsorption of TA onto accessible mesopores should not be ignored.

In order to investigate the main mechanisms intervening in the adsorption of TA on SS as function of time. The following kinetic models were used in this study: Pseudo-first-order Equation (6), Pseudo-second-order Equation (7), Elovich Equation (8), and Intra-particle models Equation (9).

$$\ln(q_e - q_t) = \ln q_e - K_1 t \quad (6)$$

where, q_e ($\text{mg}\cdot\text{g}^{-1}$) represents adsorption amount of TA at equilibrium; q_t ($\text{mg}\cdot\text{g}^{-1}$) adsorption amount at time t ; K_1 ($1\cdot\text{min}^{-1}$) pseudo-first-order rate constant.

$$\frac{t}{q_t} = \frac{1}{K_2 \cdot q_e^2} + \frac{t}{q_e} \quad (7)$$

where q_e ($\text{mg}\cdot\text{g}^{-1}$) is the adsorption amount of TA at equilibrium; q_t ($\text{mg}\cdot\text{g}^{-1}$) refers to TA absorbed onto SS at time t ; K_1 ($1\cdot\text{min}^{-1}$) represents the constant of pseudo-first-order rate, K_2 ($\text{g}\cdot\text{m}^{-1}\cdot\text{min}^{-1}$) represents the constant of pseudo-second-order rate

$$qt = \frac{1}{\beta} \ln(\alpha\beta) + \frac{1}{\beta} \ln t \quad (8)$$

where α refers to the initial adsorption coefficient ($\text{mg}\cdot\text{g}^{-1}\cdot\text{min}^{-1}$); β is the desorption coefficient ($\text{g}\cdot\text{mg}^{-1}$);

$$qt = K_{int} \sqrt{t} + C \quad (9)$$

K_{int} the constant of the rate ($\text{g}\cdot\text{mg}^{-1}\cdot\text{min}^{-1/2}$) and C is a constant of intra-particle diffusion model.

Figure 7 displays the fitting results of the four studied models. According to the fitting parameters in Table 5, the pseudo-second-order model provides the most significant correlation coefficients ($R^2 = 0.997$). According to these characteristics, the pseudo-second-order kinetic model was more accurate and helpful in simulating TA adsorption on steel slag. Considering its mathematical characteristics, the pseudo-second order fitted well the experimental adsorption data in this study and the chemical kinetics provide the best correlation for the adsorption of TA on SS. The adsorption process, known as chemisorption, chemically controls the rate-determining step of the sorption process and kinetically provides the highest correlation due to the mathematical characteristics of the pseudo-second-order model. Furthermore, a study on the adsorption of OMWW phenolic compounds onto local natural clay showed that chemisorption was mainly the governing process of adsorption and followed the pseudo-second-order [72]. Among the remaining models, the Elovich kinetic model showed in turn, a good correlation coefficient of 0.9841, confirming thus the chemical nature of TA sorption on SS.

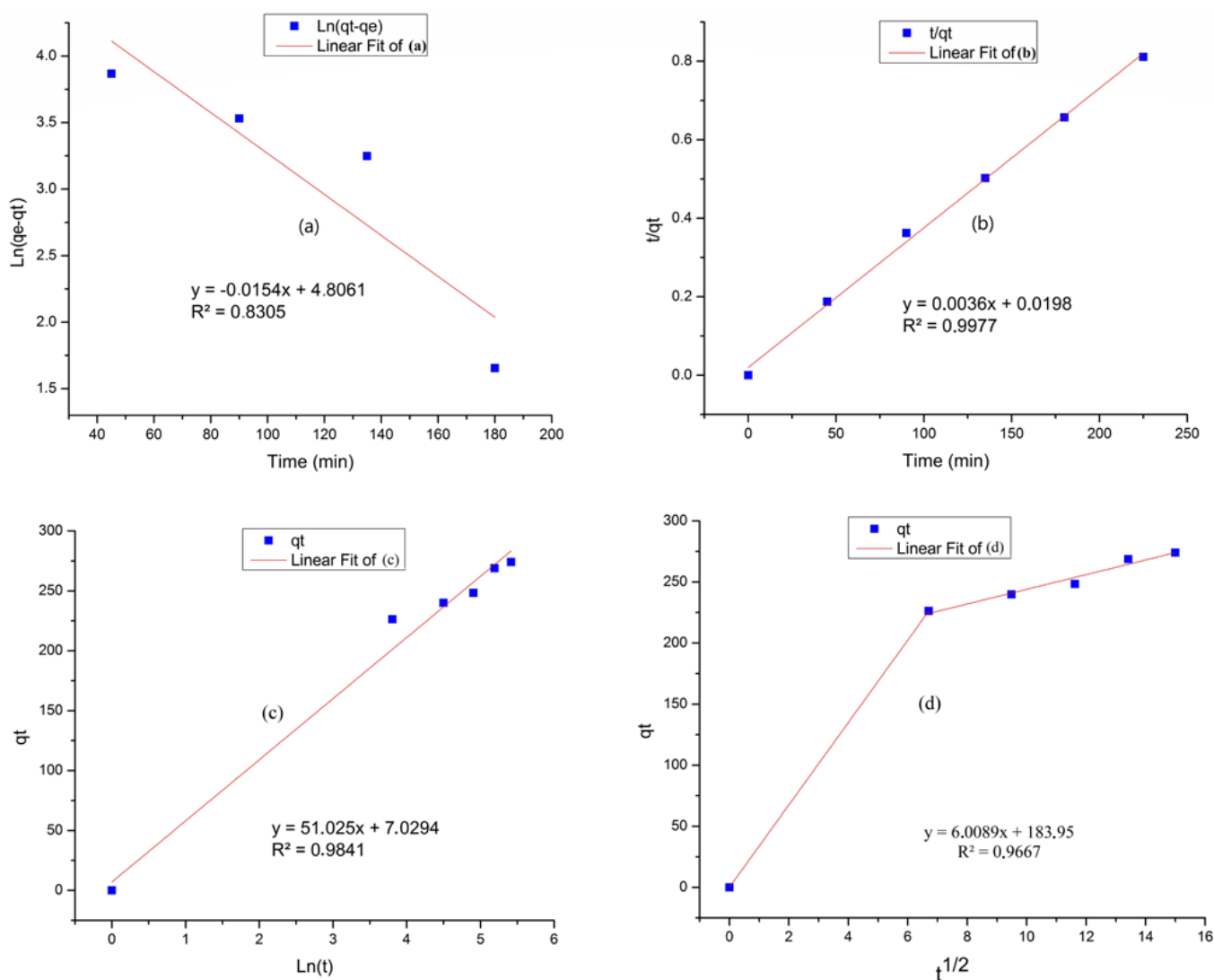


Figure 7. Kinetics curves for the TA adsorption by SS: (a–c) pseudo-first-order, pseudo-second-order and Elovich kinetics fitting, respectively, and (d) intraparticle diffusion model. Adsorption conditions: pH = 6.6; T = 293 K; time = 225 min.

Table 5. Fitting parameters of TA adsorption to SS following pseudo-first-order, pseudo-second-order, Elovich kinetics, and Intraparticle diffusion model.

Models	Pseudo-First-Order			Pseudo-Second-Order			Elovich			Intraparticle Diffusion		
Parameters	qe	K ₁	R ²	qe	K ₂	R ²	α	β	R ²	Ki	C	R ²
Value	241.048	0.0222	0.8305	294.117	1.92 10 ⁻⁴	0.9977	58.545	0.0196	0.9841	17.649	44.122	0.8496

3.4.2. Effect of SS Dosage on Adsorption of TA

In order to investigate the adsorption amount % and adsorption capacity qe (mg/g) of SS, the effect of adsorbent dosage on TA adsorption within a range of 0.5 g/L to 10 g/L of SS was investigated. In this experiment, the initial TA concentration was 300 mg/L. Figure 8 shows the removal of TA according to SS adsorbed amount (a) and adsorption capacity (b). It was observed that increasing the dosage of SS from 50 mg to 1000 mg resulted in an increased TA removal rate from 80.50% to 98.91 %, respectively. This result indicates that a small dose of adsorbent might not achieve the equilibrium adsorption of TA on SS. However, in terms of efficiency, the adsorption capacity (qe) of SS decreased

parallely with increased SS dosage at fixed TA concentration, indicating that higher SS dosage affects the adsorption capacity of TA. According to these findings, 1 g/L of SS, which demonstrates a higher removal rate of 92 %, was selected to investigate the effect of pH and initial concentrations on TA adsorption.

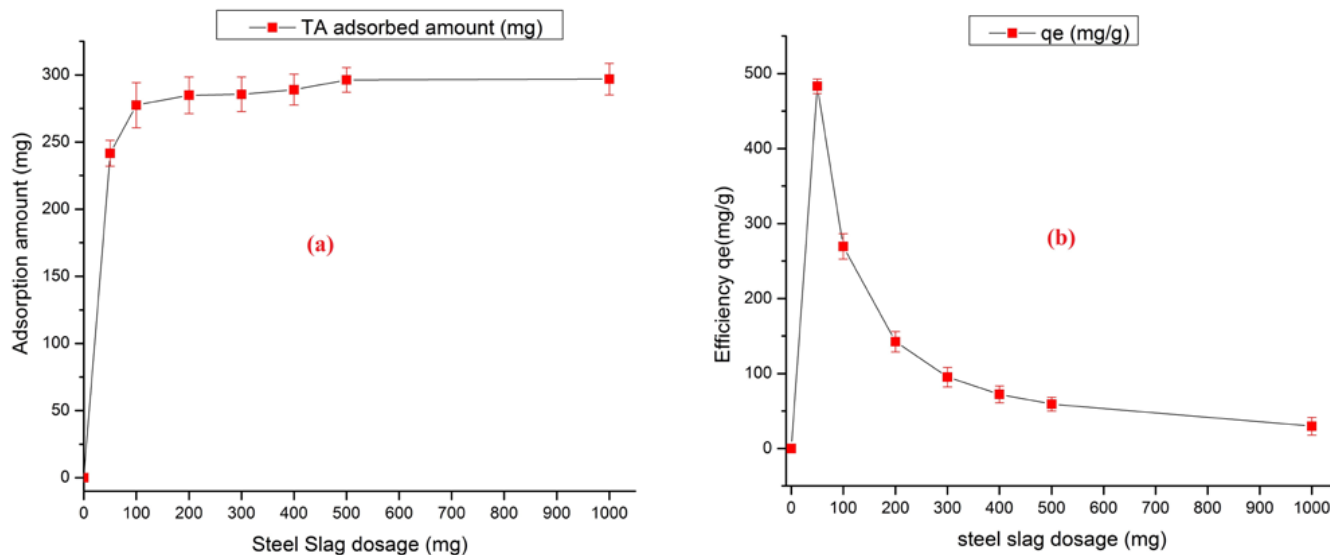


Figure 8. Effect of SS dosage on TA adsorbed amount (a) and efficiency of removal (b). Adsorption conditions: pH = 6.6; T = 293 K; time = 225 min; initial concentration = 300 mg/L, volume = 100 mL.

3.4.3. Effect of pH

The initial pH is one of the main factors influencing the adsorption behavior. As mentioned before, steel slag has high alkalinity due to its high concentration of basic oxides, which allows it to neutralize strong acids. The adsorption of TA on SS at different pH is shown in Figure 9. The results indicate that the adsorption of TA increased slightly with increasing pH values. Whereas a maximum adsorption capacity was achieved at pH 11. Generally, the transition between acidic and alkaline pH has no significant effect on TA adsorption, indicating only a slight removal difference of 5.43%. This low difference could be explained by the overdominance of the SS hydroxyl group (OH^-) in the solution, allowing the maintenance of an alkaline pH medium. It is assumed that the free cations in the solution react with the negatively charged TA molecules to create a precipitate, therefore removing TA from the aqueous solution. According to research, steel slag was able to raise the pH of acidic wastewater, thus reaching the solubility product (K_{sp}) of the contaminant and resulting in the formation of a precipitate easily separated from wastewater. A similar study reported that removing total phenolic compounds by olive pomace-activated carbon was greatly achieved at pH 10 [73]. Similarly, the adsorption of organic acids onto clay was greatly affected by higher pH and/or $\text{Ca}(\text{OH})_2$ concentration [74]. Furthermore, polyphenol dissociation can occur only when the pH of the solution is greater than the Pka of the polyphenols [75]. Given that TA Pka is approximately 6, it was evident that SS had a significant influence on TA solubility, paving the path for the adsorption process. In accordance with the findings of this investigation regarding the influence of SS on raw OMWW, and because the adsorption study is intended to evaluate the SS capacity to reduce polyphenolic substances, it is possible to infer that the amount of steel slag could be the main pH regulating agent when treating OMWW.

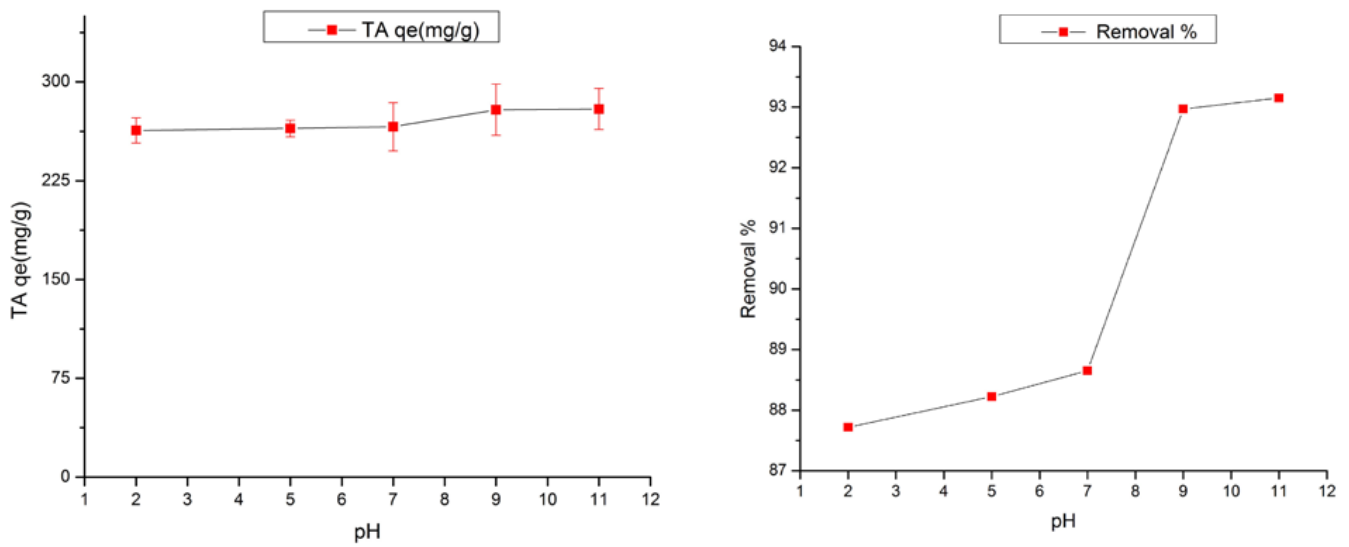


Figure 9. Effect of pH on TA adsorption. Adsorption conditions: SS dosage = 100 mg; T = 293 K; time = 225 min; initial concentration = 300 mg/L, volume = 100 mL.

3.4.4. Effect of TA Initial Concentration and Isothermal Study

The adsorption of TA on SS at different initial concentrations (50–1000 mg/L) was investigated in this study. TA adsorption according to different equilibrium concentrations (C_e) is presented in Figure 10. An apparent linearity was observed regarding the removal of tannic acid, indicating a substantial removal of more than 90 % for each investigated initial TA concentration. These results demonstrate that the adsorption capacity increases with increasing TA initial concentration. The higher initial concentrations of TA could increase the driving force required to overcome the mass transfer barrier of phenols between the liquid and solid phases, resulting in a more significant possibility of contact between TA and sorbent [75,76].

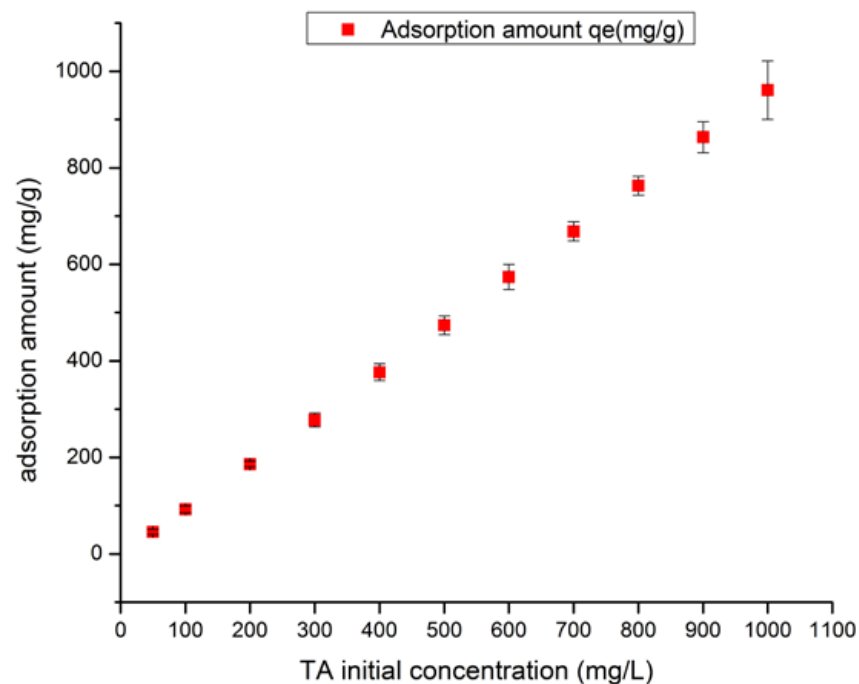


Figure 10. Adsorption isotherm of TA on SS as function of initial concentrations. Adsorption conditions: pH = 6.6; T = 293 K; time = 225 min; SS dosage = 100 mg, volume = 100 mL.

Currently, several theoretical models have been developed to describe adsorption isotherms, gathering information on surface adsorption, and types of interaction between Sorbent and Sorbate. Langmuir and Freundlich models listed below were used to model the experimental results in this study. The experimental data obtained from initial concentration were used to fit linear equation of Langmuir [77] (Equation (10)) and Freundlich [78] (Equation (11)) isotherms:

$$\text{Ln}(q_e - q_t) = \text{Ln}q_e - K_1t \tag{10}$$

$$\frac{t}{q_t} = \frac{1}{K_2 \cdot q_e^2} + \frac{t}{q_e} \tag{11}$$

where q_{max} ($\text{mg} \cdot \text{g}^{-1}$) is the Langmuir maximum adsorption capacity; C_e ($\text{mg} \cdot \text{L}^{-1}$) is the equilibrium concentration of the TA solution; q_e ($\text{mg} \cdot \text{g}^{-1}$) is the amount of TA adsorbed at equilibrium; K_L ($\text{L} \cdot \text{mg}^{-1}$) is the Langmuir bonding term related to the interaction energies, K_F ($\text{L} \cdot \text{mg}^{-1}$) is the Freundlich affinity coefficient; n is Freundlich linearity constant.

The results presented in Table 6 summarizes the different constants obtained for each model, according to the Langmuir and Freundlich plotting models Figure 11.

Table 6. Parameters of the Freundlich and Langmuir models for TA adsorption on steel slag.

Types	Langmuir Isotherm				Freundlich Isotherm		
Parameter	q_{max} ($\text{mg} \cdot \text{g}^{-1}$)	K_L ($\text{L} \cdot \text{mg}^{-1}$)	R_L	R^2	K_F ($\text{L} \cdot \text{mg}^{-1}$)	$1/n$	R^2
Value	714.28	0.01380	0.59	0.9969	9.76	0.6906	0.9782

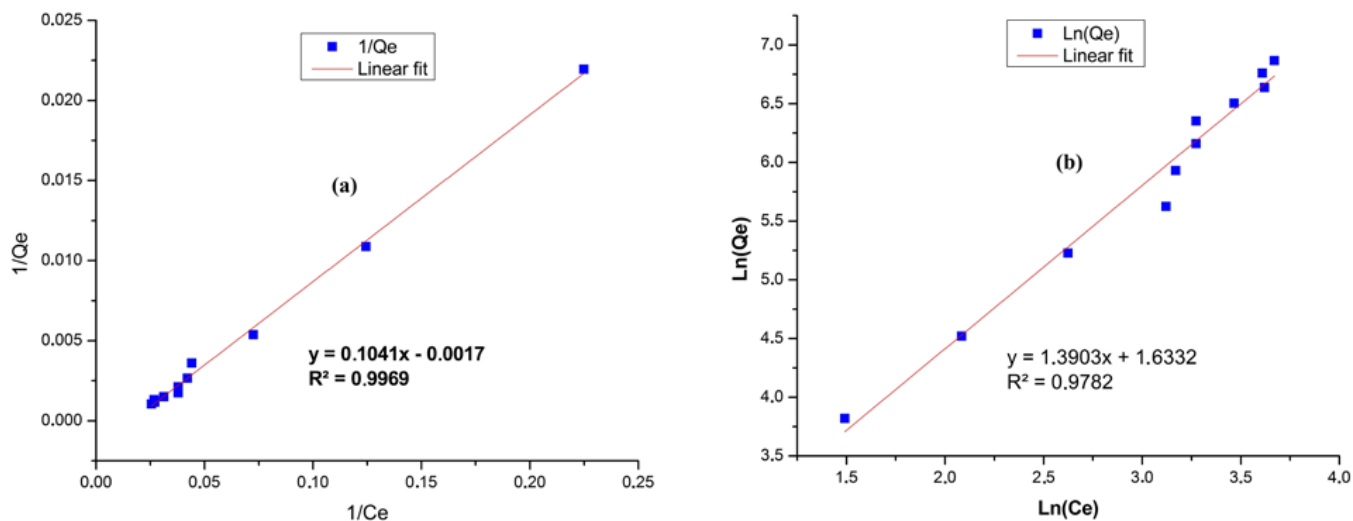


Figure 11. Adsorption isotherm for the TA adsorption by Steel Slag: Langmuir (a), Freundlich (b).

According to the fitting results, the Langmuir isotherm provides higher correlation coefficient to experimental data $R = 0.9969$, while a significant correlation was also observed by Freundlich model displaying a coefficient of $R = 0.9782$. These findings indicate that the adsorption of TA on SS conforms suitably to both Langmuir and Freundlich models. The assumption regarding Langmuir’s model is that TA adsorption occurs on a homogeneous monolayer surface of SS with no interaction between adsorbed molecules. Previous studies have shown that TA adsorption onto polyaniline [25], commercial resins XAD-7, XAD-4, and NDA-7 [24], surfactant-modified zeolite [79], chitosan-coated attapulgite [33], chitosan/NaOH/fly ash [80], soy protein isolate–alginate hybrid spheres (SPIAHS) [81], and green synthesized nano-hydroxyapatite [82], has similar affinity for the Langmuir model reporting a $q(\text{max})$ values of 1023, 286, 111, 95.2, 286, 243.90, 1076.5, and 94.8 mg/g , respectively. According to Shi et al., the Langmuir model may adequately represent the adsorption process of numerous pollutants onto SS [39]. In this study, the maximum adsorption capac-

ity (q_{\max}) of SS following the Langmuir model was 714.28 (mg/g), indicating a promising adsorption capacity when compared to the aforementioned synthesized adsorbents.

The separation factor (RL) shows whether the form of the isotherms is unfavorable ($RL > 1$), linear ($RL = 1$), favorable ($0 < RL < 1$), or irreversible ($RL = 0$). The calculated RL parameter was 0.59, implying that the adsorption of TA on SS was favorable.

3.4.5. Adsorption Thermodynamics

The thermodynamic parameters of free energy change (ΔG_0), enthalpy change (ΔH_0), and entropy change (ΔS_0), might be valuable in gathering further information on the thermodynamic adsorption behavior of TA on steel slag. The parameters were calculated using Equations (12)–(14):

$$\Delta G^\circ = -RT\ln(K_d) \text{ and } \Delta G^\circ = \Delta H^\circ - T\Delta S^\circ \quad (12)$$

$$\ln(K_d) = \frac{\Delta S^\circ}{R} - \frac{\Delta H^\circ}{RT} \quad (13)$$

$$K_d = \frac{Q_e}{C_e} \quad (14)$$

where: T is the temperature in kelvin (K); K_d is the distribution constant in ($l \cdot g^{-1}$); R is the gas constant ($8.314 \text{ J} \cdot \text{mol}^{-1} \cdot \text{K}^{-1}$).

The thermodynamic equilibrium constant was calculated by plotting $\ln(q_e/C_e)$ vs q_e (Figure 12). ΔH° and ΔS° were determined from the slope and intercept of $\ln(q_e/C_e)$ vs. $1/T$ plotting. The results reported in Table 7 show a positive value of ΔH° , suggesting an endothermic mechanism for TA adsorption on SS. This is supported by the fact that increasing the temperature decreases TA concentration in the solution. In addition, the absolute value of ΔH° was 5.5 kJ/mol, demonstrating that hydrogen bonding intervenes in the adsorption process of TA in steel slag [81]. The negative value ΔG° suggests that the adsorption occurred spontaneously. The decrease in ΔG_0 as temperature increases suggests that higher removal rates could be achieved in higher temperatures. The high positive value of ΔS° ($33.38 \text{ J} \cdot \text{mol}^{-1} \cdot \text{K}^{-1}$) indicates that TA adsorption on SS is an entropy-increasing mechanism that is traduced by the higher degree of freedom of TA and its affinity of SS surface.

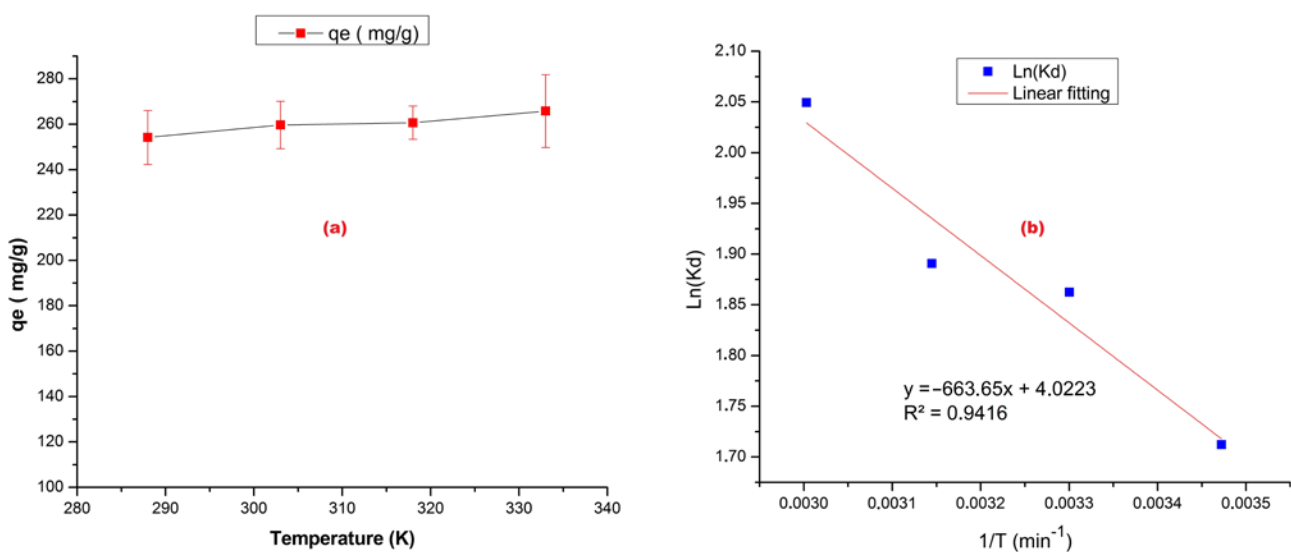


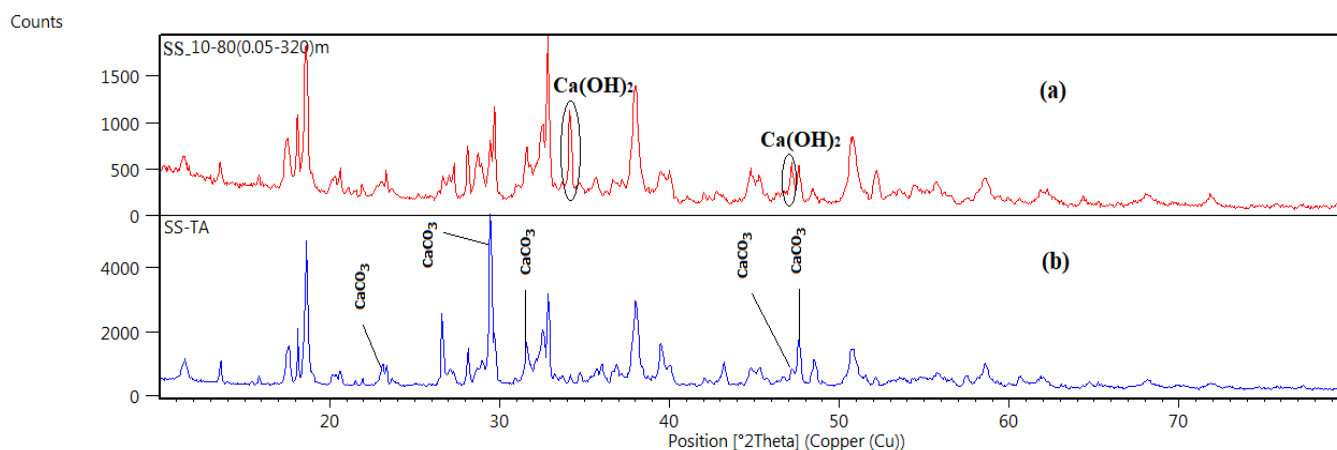
Figure 12. Effect of temperature on the adsorption of TA by steel slag ($C_0 = 300 \text{ mg/L}$; $m = 100 \text{ mg}$; $V = 100 \text{ mL}$; $\text{pH} = 6.6 \pm 0.1$; time = 225 min; Agitation = 500 rpm) (a), adsorption thermodynamic for the TA adsorption by steel slag (b).

Table 7. Thermodynamics parameters for the adsorption of acid tannic on steel slag.

Thermodynamic Parameters	ΔG° (kJ·mol ⁻¹)				ΔH° (kJ·mol ⁻¹)	ΔS° (J·mol ⁻¹ ·K ⁻¹)
	288	303	318	333		
Temperature	288	303	318	333		
Value	−4.107	−4.608	−5.108	−5.776	5.506	33.3798

3.5. Characterization of SS–TA before Adsorption

In order to explore the SS-loaded TA characteristics after adsorption, XRD patterns of raw SS and SS-loaded TA were compared in Figure 13. By comparing the peaks characteristics, it was observed that calcite CaCO₃ phase was appeared in the SS–TA composition, noting that no calcium carbonate phase was detected in the raw SS. On the other hand, calcium hydroxide Ca(OH)₂ peaks were reduced after the adsorption of TA onto SS. The precipitation of TA in water solution and subsequent formation of CaCO₃ may be attributed to the interaction of the TA carbon molecules (C₇₆H₅₂O₄₆) with calcium hydroxide Ca(OH)₂. It was also noticed that SS composition after TA adsorption was approximately the same structure as before adsorption. Zhao et al. [83] compared the steel slag XRD characteristics before and after adsorption of p-Nitrophenol and reported no significant changes in the crystalline phase of SS. Similarly, the same authors indicated the reduction in Ca(OH)₂ and Ca₂SiO₄ peaks after adsorption. The significant difference in peaks intensities before and after adsorption suggests that TA could affect the crystalline size of SS resulting in higher and sharper peaks. In addition, since the material maintains approximately the same structure as before adsorption the potential of its reuse still possible. Among the techniques suggested is pyrolysis of SS-loaded TA to remove TA organic carbon. This regeneration procedure could result in a great substance with a larger surface area that can be reused in other applications.

**Figure 13.** XRD patterns of raw steel slag after adsorption (a), and SS–TA before adsorption (b).

Significant differences between the raw SS and SS-loaded TA were observed by scanning electron microscopy (Figure 14). It can be seen that there was in fact a reaction between the TA and the SS surface functions (micrograph f). The raw SS showed sharp edges composed mainly from different shapes (micrographs a–c). The surface morphology of TA-adsorbed SS, on the other hand, differed from that of SS, as evidenced by a decrease in SS cracks and mesopores. After the adsorption, the SS-loaded TA showed a relatively rounded structure on which a thin carbon coating layer has been developed. This thin layer was characterized by a woolly texture covering the surface of SS (micrographs d,e). These findings demonstrated that TA molecules were well adsorbed onto the surface of SS.

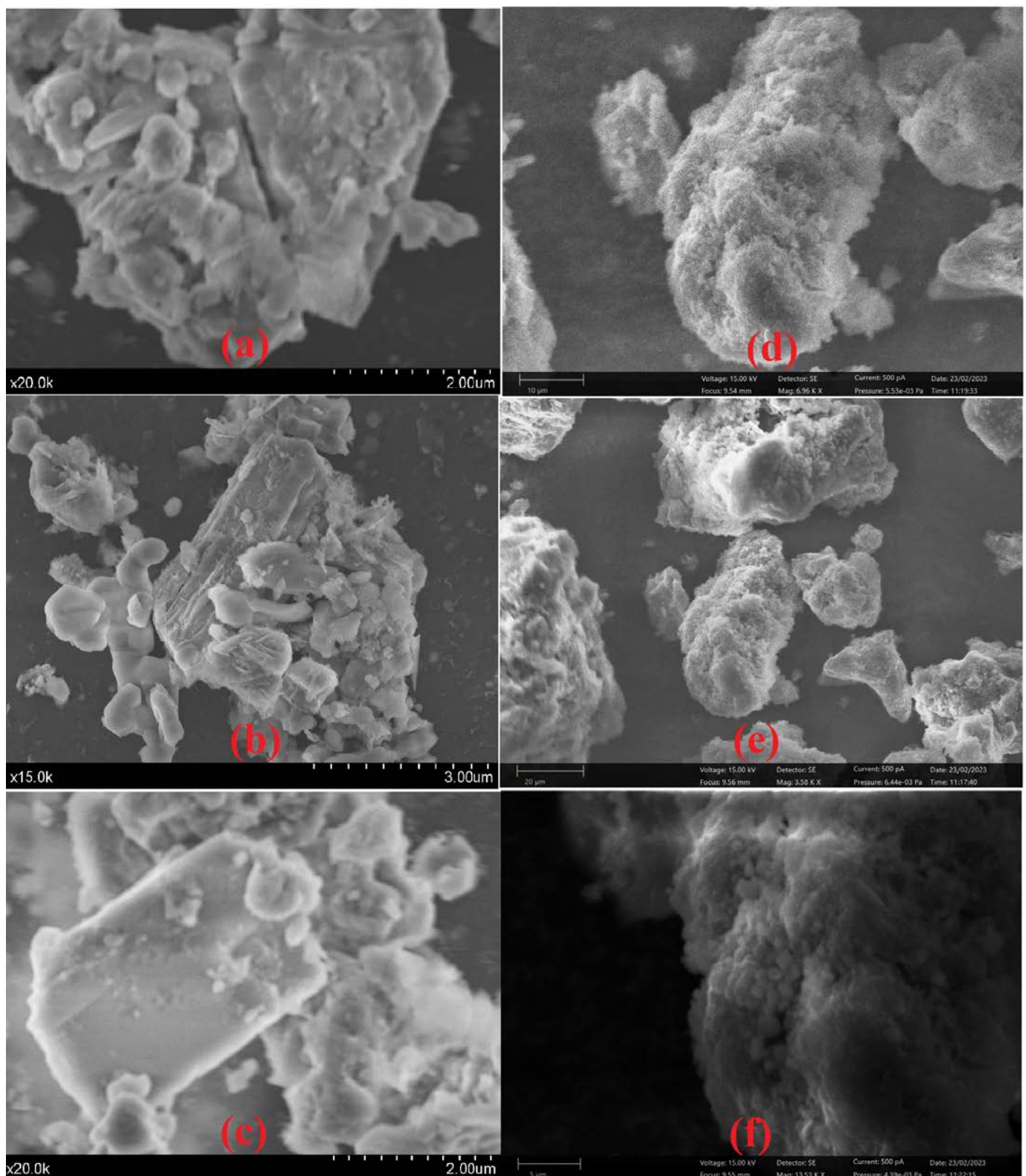


Figure 14. Scanning electron microscope (SEM) of SS before adsorption (a–c), and SS-loaded TA after adsorption (d–f).

4. Conclusions

In this study the potential treatment of olive mill wastewater (OMWW) by steel slag (SS) as an improver and adsorbent was investigated. The OMWW characterization demonstrated that this effluent is acidic, rich in organic matter and polyphenols, and displayed

higher chemical and biological oxygen demands, whereas SS characterization showed that this residue is non-toxic, rich in alkaline metals oxides and hydroxides, and possesses a meso-macroporous structure, which provides an excellent material to be valorized in wastewater treatment.

The buffer capacity of SS was investigated in order to promote neutral disposal conditions of OMWW. The results confirm that SS could be used as a liming material, given its high content in alkaline oxyhydroxides. Moreover, the neutralization process could be achieved by controlling the optimal SS dosage in the function of time. In addition, the OMWW neutralization by SS might be responsible for reducing COD and phytotoxic polyphenols.

The study of tannic Acid (TA) adsorption onto steel slag (SS) was carried out to assess the SS capacity in reducing the total polyphenolic compounds in OMWWs. The following points were the main conclusions:

Batch experiments revealed that an alkaline medium could be a favorable sorption condition for TA on SS.

The maximum adsorption efficiency can reach 98.91% with an adsorbent dosage of 10 g/L. However, a decrease in adsorption efficiency was related to higher SS dosages.

The TA adsorption increased with the contact time until reaching the equilibrium which was higher than 90 % of initial TA concentrations, indicating that the adsorption capacity increased while increasing the initial TA concentration.

The adsorption capacity increased with increasing the temperature.

Adsorption kinetic and mechanism investigations revealed that TA adsorption fitted the pseudo-second-order kinetic model and Elovich. While Langmuir, isotherm described the TA adsorption on SS suitably, providing a maximum adsorption capacity (q_{max}) of 714.28 mg/g.

The chemical alterations in SS resulting from the interactions between SS and TA chemical bonds were emphasized by the characterization of SS after TA adsorption. The affinity towards Langmuir and pseudo-second-order models observed during the TA adsorption on SS indicate that chemisorption was the mechanism underlying TA adsorption onto SS.

This study shows that steel slag, an industrial waste, is a low-cost and readily accessible adsorbent for treating OMWWs. Further research should be carried out on the recovery of valuable chemicals from SS.

Author Contributions: Conceptualization, O.S. and F.E.M.; methodology, O.S.; software, O.S.; validation, O.S., F.E.M. and M.S.; formal analysis, J.M.; investigation, O.S. and E.H.Y.; resources, F.E.M., E.O. and M.S.; writing—original draft preparation, O.S. and F.E.M.; writing—review and editing, E.O., J.M. and F.E.M.; visualization, J.M.; supervision, M.S.; project administration, M.S. All authors have read and agreed to the published version of the manuscript.

Funding: This research received no external funding.

Institutional Review Board Statement: Not applicable.

Informed Consent Statement: Not applicable.

Data Availability Statement: Not applicable.

Acknowledgments: The authors are thankful to Mustapha EL HADRI, for his assistance in characterizing steel slag using XRD and SEM techniques after adsorption. The analysis was carried out in the Faculty of Sciences, University Abdelmalek Essaâdi, Tetouan.

Conflicts of Interest: The authors declare no conflict of interest.

References

1. Lechhab, T.; Lechhab, W.; Cacciola, F.; Salmoun, F. Sets of Internal and External Factors Influencing Olive Oil (*Olea europaea* L.) Composition: A Review. *Eur. Food Res. Technol.* **2022**, *248*, 1069–1088. [[CrossRef](#)]
2. Lechhab, T.; Salmoun, F.; Lechhab, W.; El Majdoub, Y.O.; Russo, M.; Camillo, M.R.T.; Trovato, E.; Dugo, P.; Mondello, L.; Cacciola, F. Determination of Bioactive Compounds in Extra Virgin Olive Oils from 19 Moroccan Areas Using Liquid Chromatography Coupled to Mass Spectrometry: A Study over Two Successive Years. *Eur. Food Res. Technol.* **2021**, *247*, 2993–3012. [[CrossRef](#)]
3. Lechhab, W.; Cincotta, F.; Lechhab, T.; Conurso, C.; Salmoun, F.; Cacciola, F.; Verzera, A. Preliminary Assessment of Occurrence, Potential Origin, and Human Health Risk of Volatile Organic Compounds in Uncontrolled Springs, North Morocco. *Metabolites* **2022**, *12*, 1213. [[CrossRef](#)]
4. Alaoui, S.; Aissam, H.; Merzouki, M.; Benlemlih, M. Characterization of the Harmful Effect of Olive Mill Wastewater on Spearmint. *J. Hazard Mater.* **2009**, *170*, 779–785.
5. Baniyas, G.; Achillas, C.; Vlachokostas, C.; Moussiopoulos, N.; Stefanou, M. Environmental Impacts in the Life Cycle of Olive Oil: A Literature Review. *J. Sci. Food Agric.* **2017**, *97*, 1686–1697. [[CrossRef](#)]
6. Scioli, C.; Vollaro, L. The Use of *Yarrowia lipolytica* to Reduce Pollution in Olive Mill Wastewaters. *Water Res.* **1997**, *31*, 2520–2524. [[CrossRef](#)]
7. Tsioulpas, A.; Dimou, D.; Iconomou, D.; Aggelis, G. Phenolic Removal in Olive Oil Mill Wastewater by Strains of *Pleurotus* spp. in Respect to Their Phenol Oxidase (Laccase) Activity. *Bioresour. Technol.* **2002**, *84*, 251–257. [[CrossRef](#)]
8. Khdaif, A.I.; Abu-Rumman, G.; Khdaif, S.I. Pollution Estimation from Olive Mills Wastewater in Jordan. *Heliyon* **2019**, *5*, e02386. [[CrossRef](#)]
9. El Hassani, F.Z.; Fadile, A.; Faouzi, M.; Zinedine, A.; Merzouki, M.; Benlemlih, M. The Long Term Effect of Olive Mill Wastewater (OMW) on Organic Matter Humification in a Semi-Arid Soil. *Heliyon* **2020**, *6*, e03181. [[CrossRef](#)]
10. Elabdouni, A.; Haboubi, K.; Merimi, I.; El Youbi, M.S.M. Olive Mill Wastewater (OMW) Production in the Province of Al-Hoceima (Morocco) and Their Physico-Chemical Characterization by Mill Types. *Mater. Today Proc.* **2020**, *27*, 3145–3150. [[CrossRef](#)]
11. Eroğlu, E.; Eroğlu, İ.; Gündüz, U.; Yücel, M. Treatment of Olive Mill Wastewater by Different Physicochemical Methods and Utilization of Their Liquid Effluents for Biological Hydrogen Production. *Biomass Bioenergy* **2009**, *33*, 701–705. [[CrossRef](#)]
12. Ginos, A.; Manios, T.; Mantzavinos, D. Treatment of Olive Mill Effluents by Coagulation–Flocculation–Hydrogen Peroxide Oxidation and Effect on Phytotoxicity. *J. Hazard. Mater.* **2006**, *133*, 135–142. [[CrossRef](#)]
13. Jaouani, A.; Vanthourhout, M.; Penninckx, M.J. Olive Oil Mill Wastewater Purification by Combination of Coagulation–Flocculation and Biological Treatments. *Environ. Technol.* **2005**, *26*, 633–642. [[CrossRef](#)] [[PubMed](#)]
14. Michael, I.; Panagi, A.; Ioannou, L.A.; Frontistis, Z.; Fatta-Kassinos, D. Utilizing Solar Energy for the Purification of Olive Mill Wastewater Using a Pilot-Scale Photocatalytic Reactor after Coagulation–Flocculation. *Water Res.* **2014**, *60*, 28–40. [[CrossRef](#)] [[PubMed](#)]
15. Papaphilippou, P.C.; Yiannapas, C.; Politi, M.; Daskalaki, V.M.; Michael, C.; Kalogerakis, N.; Mantzavinos, D.; Fatta-Kassinos, D. Sequential Coagulation–Flocculation, Solvent Extraction and Photo-Fenton Oxidation for the Valorization and Treatment of Olive Mill Effluent. *Chem. Eng. J.* **2013**, *224*, 82–88. [[CrossRef](#)]
16. Inan, H.; Dimoglo, A.; Şimşek, H.; Karpuzcu, M. Olive Oil Mill Wastewater Treatment by Means of Electro-Coagulation. *Sep. Purif. Technol.* **2004**, *36*, 23–31. [[CrossRef](#)]
17. Pelendridou, K.; Michailides, M.K.; Zagklis, D.P.; Tekerlekopoulou, A.G.; Paraskeva, C.A.; Vayenas, D. V Treatment of Olive Mill Wastewater Using a Coagulation–Flocculation Process Either as a Single Step or as Post-treatment after Aerobic Biological Treatment. *J. Chem. Technol. Biotechnol.* **2014**, *89*, 1866–1874. [[CrossRef](#)]
18. Marques, I.P. Anaerobic Digestion Treatment of Olive Mill Wastewater for Effluent Re-Use in Irrigation. *Desalination* **2001**, *137*, 233–239. [[CrossRef](#)]
19. Yangui, A.; Abderrabba, M. Towards a High Yield Recovery of Polyphenols from Olive Mill Wastewater on Activated Carbon Coated with Milk Proteins: Experimental Design and Antioxidant Activity. *Food Chem.* **2018**, *262*, 102–109. [[CrossRef](#)]
20. Abu-Dalo, M.; Abdelnabi, J.; Bawab, A. Al Preparation of Activated Carbon Derived from Jordanian Olive Cake and Functionalized with Cu/Cu₂O/CuO for Adsorption of Phenolic Compounds from Olive Mill Wastewater. *Materials* **2021**, *14*, 6636. [[CrossRef](#)]
21. Pepi, M.; Lampariello, L.R.; Altieri, R.; Esposito, A.; Perra, G.; Renzi, M.; Lobianco, A.; Feola, A.; Gasperini, S.; Focardi, S.E. Tannic Acid Degradation by Bacterial Strains *Serratia* Spp. and *Pantoea* Sp. Isolated from Olive Mill Waste Mixtures. *Int. Biodeterior. Biodegrad.* **2010**, *64*, 73–80. [[CrossRef](#)]
22. Wang, J.; Zheng, C.; Ding, S.; Ma, H.; Ji, Y. Behaviors and Mechanisms of Tannic Acid Adsorption on an Amino-Functionalized Magnetic Nanoadsorbent. *Desalination* **2011**, *273*, 285–291. [[CrossRef](#)]
23. Wang, J.; Zheng, S.; Liu, J.; Xu, Z. Tannic Acid Adsorption on Amino-Functionalized Magnetic Mesoporous Silica. *Chem. Eng. J.* **2010**, *165*, 10–16. [[CrossRef](#)]
24. Wang, J.; Li, A.; Xu, L.; Zhou, Y. Adsorption of Tannic and Gallic Acids on a New Polymeric Adsorbent and the Effect of Cu (II) on Their Removal. *J. Hazard. Mater.* **2009**, *169*, 794–800. [[CrossRef](#)] [[PubMed](#)]
25. Sun, C.; Xiong, B.; Pan, Y.; Cui, H. Adsorption Removal of Tannic Acid from Aqueous Solution by Polyaniline: Analysis of Operating Parameters and Mechanism. *J. Colloid Interface Sci.* **2017**, *487*, 175–181. [[CrossRef](#)]
26. Mansouri, K.; Elsaid, K.; Bedoui, A.; Bensalah, N.; Abdel-Wahab, A. Application of Electrochemically Dissolved Iron in the Removal of Tannic Acid from Water. *Chem. Eng. J.* **2011**, *172*, 970–976. [[CrossRef](#)]
27. Jung, C.; Phal, N.; Oh, J.; Chu, K.H.; Jang, M.; Yoon, Y. Removal of Humic and Tannic Acids by Adsorption–Coagulation Combined Systems with Activated Biochar. *J. Hazard. Mater.* **2015**, *300*, 808–814. [[CrossRef](#)] [[PubMed](#)]

28. Ulbricht, M.; Ansorge, W.; Danielzik, I.; König, M.; Schuster, O. Fouling in Microfiltration of Wine: The Influence of the Membrane Polymer on Adsorption of Polyphenols and Polysaccharides. *Sep. Purif. Technol.* **2009**, *68*, 335–342. [[CrossRef](#)]
29. Afify, A.S.; Mahmoud, M.A.; Emara, H.A.; Abdelkreem, K.I. Phenolic Compounds and COD Removal from Olive Mill Wastewater by Chemical and Biological Procedures. *Aust. J. Basic Appl. Sci.* **2009**, *3*, 1087–1095.
30. Lin, D.; Xing, B. Tannic Acid Adsorption and Its Role for Stabilizing Carbon Nanotube Suspensions. *Environ. Sci. Technol.* **2008**, *42*, 5917–5923. [[CrossRef](#)]
31. Zhang, W.; Yang, Z.-Y.; Cheng, X.-W.; Tang, R.-C.; Qiao, Y.-F. Adsorption, Antibacterial and Antioxidant Properties of Tannic Acid on Silk Fiber. *Polymers* **2019**, *11*, 970. [[CrossRef](#)] [[PubMed](#)]
32. Li, J.; Ma, S.; Li, X.; Wei, W. Adsorption of Tannic Acid and Macromolecular Humic/Fulvic Acid onto Polystyrene Microplastics: A Comparison Study. *Water* **2022**, *14*, 2201. [[CrossRef](#)]
33. Teng, Y.; Liu, Z.; Yao, K.; Song, W.; Sun, Y.; Wang, H.; Xu, Y. Preparation of Attapulgit/CoFe₂O₄ Magnetic Composites for Efficient Adsorption of Tannic Acid from Aqueous Solution. *Int. J. Environ. Res. Public Health* **2019**, *16*, 2187. [[CrossRef](#)] [[PubMed](#)]
34. An, J.-H.; Dultz, S. Adsorption of Tannic Acid on Chitosan-Montmorillonite as a Function of PH and Surface Charge Properties. *Appl. Clay Sci.* **2007**, *36*, 256–264. [[CrossRef](#)]
35. Chang, M.-Y.; Juang, R.-S. Adsorption of Tannic Acid, Humic Acid, and Dyes from Water Using the Composite of Chitosan and Activated Clay. *J. Colloid Interface Sci.* **2004**, *278*, 18–25. [[CrossRef](#)]
36. Jevremović, A.; Božinović, N.; Arsenijević, D.; Marmakov, S.; Vasiljević, B.N.; Uskoković-Marković, S.; Bajuk-Bogdanović, D.; Milojević-Rakić, M. Modulation of Cytotoxicity by Consecutive Adsorption of Tannic Acid and Pesticides on Surfactant Functionalized Zeolites. *Environ. Sci. Process. Impacts* **2020**, *22*, 2199–2211. [[CrossRef](#)] [[PubMed](#)]
37. Yüksel, İ. A Review of Steel Slag Usage in Construction Industry for Sustainable Development. *Environ. Dev. Sustain.* **2017**, *19*, 369–384. [[CrossRef](#)]
38. Jiang, Y.; Ahmad, M.R.; Chen, B. Properties of Magnesium Phosphate Cement Containing Steel Slag Powder. *Constr. Build. Mater.* **2019**, *195*, 140–147. [[CrossRef](#)]
39. Shi, C.; Wang, X.; Zhou, S.; Zuo, X.; Wang, C. Mechanism, Application, Influencing Factors and Environmental Benefit Assessment of Steel Slag in Removing Pollutants from Water: A Review. *J. Water Process. Eng.* **2022**, *47*, 102666. [[CrossRef](#)]
40. Miyata, Y.; Hayashi, A.; Kuwayama, M.; Yamamoto, T.; Urabe, N. Reduction Test of Hydrogen Sulfide in Silty Sediment of Fukuyama Inner Harbor Using Steelmaking Slag. *ISIJ Int.* **2015**, *55*, 2686–2693. [[CrossRef](#)]
41. Scott, I.S.P.C.; Penn, C.J. Estimating the Variability of Steel Slag Properties and Their Influence in Phosphorus Removal Ability. *Chemosphere* **2021**, *276*, 130205. [[CrossRef](#)]
42. Liem-Nguyen, V.; Sjöberg, V.; Dinh, N.P.; Huy, D.H.; Karlsson, S. Removal Mechanism of Arsenic (V) by Stainless Steel Slags Obtained from Scrap Metal Recycling. *J. Environ. Chem. Eng.* **2020**, *8*, 103833. [[CrossRef](#)]
43. Wang, M.; Wang, X.; Zhang, M.; Han, W.; Yuan, Z.; Zhong, X.; Yu, L.; Ji, H. Treatment of Cd (II) and As (V) Co-Contamination in Aqueous Environment by Steel Slag-Biochar Composites and Its Mechanism. *J. Hazard. Mater.* **2023**, *447*, 130784. [[CrossRef](#)] [[PubMed](#)]
44. Jiang, Z.; Chen, X.; Zhao, J. Quantitative Removal of Ammonia Nitrogen and Phosphorus with Compound of Zeolite and Steel Slag. *Environ. Sci. Technol. (China)* **2016**, *39*, 133–138.
45. Wang, J.; Zhong, M.; Wu, P.; Wen, S.; Huang, L.; Ning, P. A Review of the Application of Steel Slag in CO₂ Fixation. *ChemBioEng Rev.* **2021**, *8*, 189–199. [[CrossRef](#)]
46. Tian, S.; Jiang, J.; Li, K.; Yan, F.; Chen, X. Performance of Steel Slag in Carbonation–Calcination Looping for CO₂ Capture from Industrial Flue Gas. *Rsc Adv.* **2014**, *4*, 6858–6862. [[CrossRef](#)]
47. Miranda-Pizarro, J.; Perejón, A.; Valverde, J.M.; Sánchez-Jiménez, P.E.; Pérez-Maqueda, L.A. Use of Steel Slag for CO₂ Capture under Realistic Calcium-Looping Conditions. *RSC Adv.* **2016**, *6*, 37656–37663. [[CrossRef](#)]
48. Li, H.; Tang, Z.; Li, N.; Cui, L.; Mao, X. Mechanism and Process Study on Steel Slag Enhancement for CO₂ Capture by Seawater. *Appl. Energy* **2020**, *276*, 115515. [[CrossRef](#)]
49. Singleton, V.L.; Orthofer, R.; Lamuela-Raventós, R.M. [14] Analysis of Total Phenols and Other Oxidation Substrates and Antioxidants by Means of Folin-Ciocalteu Reagent. In *Methods in Enzymology*; Elsevier: Amsterdam, The Netherlands, 1999; Volume 299, pp. 152–178. ISBN 0076-6879.
50. Romeo, R.; De Bruno, A.; Imeneo, V.; Piscopo, A.; Poiana, M. Impact of Stability of Enriched Oil with Phenolic Extract from Olive Mill Wastewaters. *Foods* **2020**, *9*, 856. [[CrossRef](#)] [[PubMed](#)]
51. Niaounakis, M.; Halvadakis, C.P. *Olive Processing Waste Management: Literature Review and Patent Survey*; Elsevier: Amsterdam, The Netherlands, 2006.
52. Daässi, D.; Lozano-Sánchez, J.; Borrás-Linares, I.; Belbahri, L.; Woodward, S.; Zouari-Mechichi, H.; Mechichi, T.; Nasri, M.; Segura-Carretero, A. Olive Oil Mill Wastewaters: Phenolic Content Characterization during Degradation by *Coriopsis gallica*. *Chemosphere* **2014**, *113*, 62–70. [[CrossRef](#)]
53. Dutournié, P.; Jeguirim, M.; Khiari, B.; Goddard, M.-L.; Jellali, S. Olive Mill Wastewater: From a Pollutant to Green Fuels, Agricultural Water Source, and Bio-Fertilizer. Part 2: Water Recovery. *Water* **2019**, *11*, 768. [[CrossRef](#)]
54. El Mouddeh, H.; El Idrissi, Y.; Belmaghraoui, W.; Belhoussaine, O.; El Guezane, C.; Bouayoun, T.; Harhar, H.; Tabyaoui, M. Olive Mill Wastewater Polyphenol-based Extract as a Vegetable Oil Shelf Life Extending Additive. *J. Food Process. Preserv.* **2020**, *44*, e14990. [[CrossRef](#)]

55. Shabir, S.; Ilyas, N.; Saeed, M.; Bibi, F.; Sayyed, R.Z.; Almalki, W.H. Treatment Technologies for Olive Mill Wastewater with Impacts on Plants. *Environ. Res.* **2023**, *216*, 114399. [[CrossRef](#)] [[PubMed](#)]
56. El Gnaoui, Y.; Sounni, F.; Bakraoui, M.; Karouach, F.; Benlemlih, M.; Barz, M.; El Bari, H. Anaerobic Co-Digestion Assessment of Olive Mill Wastewater and Food Waste: Effect of Mixture Ratio on Methane Production and Process Stability. *J. Environ. Chem. Eng.* **2020**, *8*, 103874. [[CrossRef](#)]
57. Bouknana, D.; Hammouti, B.; Salghi, R.; Jodeh, S.; Zarrouk, A.; Warad, I.; Aouniti, A.; Sbaa, M. Physicochemical Characterization of Olive Oil Mill Wastewaters in the Eastern Region of Morocco. *J. Mater. Environ. Sci.* **2014**, *5*, 1039–1058.
58. Manocha, S.; Ponchon, F. Management of Lime in Steel. *Metals* **2018**, *8*, 686. [[CrossRef](#)]
59. De Martino, A.; Arienzo, M.; Iorio, M.; Vinale, F.; Lorito, M.; Prenzler, P.D.; Ryan, D.; Obied, H.K. Detoxification of Olive Mill Wastewaters by Zinc–Aluminium Layered Double Hydroxides. *Appl. Clay Sci.* **2011**, *53*, 737–744. [[CrossRef](#)]
60. Hu, R.; Xie, J.; Wu, S.; Yang, C.; Yang, D. Study of Toxicity Assessment of Heavy Metals from Steel Slag and Its Asphalt Mixture. *Materials* **2020**, *13*, 2768. [[CrossRef](#)] [[PubMed](#)]
61. Rađenović, A.; Malina, J.; Sofilić, T. Characterization of Ladle Furnace Slag from Carbon Steel Production as a Potential Adsorbent. *Adv. Mater. Sci. Eng.* **2013**, *2013*, 198240. [[CrossRef](#)]
62. Navarro, C.; Díaz, M.; Villa-García, M.A. Physico-Chemical Characterization of Steel Slag. Study of Its Behavior under Simulated Environmental Conditions. *Environ. Sci. Technol.* **2010**, *44*, 5383–5388. [[CrossRef](#)]
63. Boukhoubza, F.; Jail, A.; Korchi, F.; Idrissi, L.L.; Hannache, H.; Duarte, J.C.; Hassani, L.; Nejmeddine, A. Application of Lime and Calcium Hypochlorite in the Dephenolisation and Discolouration of Olive Mill Wastewater. *J. Environ. Manag.* **2009**, *91*, 124–132. [[CrossRef](#)]
64. Uğurlu, M.; Kula, İ. Decolourization and Removal of Some Organic Compounds from Olive Mill Wastewater by Advanced Oxidation Processes and Lime Treatment. *Environ. Sci. Pollut. Res.-Int.* **2007**, *14*, 319–325. [[CrossRef](#)]
65. Achak, M.; Ouazzani, N.; Yaacoubi, A.; Mandi, L. Modern Olive Mill Effluent Characterization and Their Treatment by Coagulation–Flocculation Using Lime and Aluminium Sulphate. *Caractérisation Des Margines Issues D'une Huilerie Mod-Erne Essais Leur Trait. Par Coagul.-Flocculation Chaux Sulfate D'aluminium* **2008**, *21*, 53–67.
66. Sağlık, S.; Ersoy, L.; İmre, S. Oil Recovery from Lime-treated Wastewater of Olive Mills. *Eur. J. Lipid Sci. Technol.* **2002**, *104*, 212–215. [[CrossRef](#)]
67. Aktas, E.S.; Imre, S.; Ersoy, L. Characterization and Lime Treatment of Olive Mill Wastewater. *Water Res.* **2001**, *35*, 2336–2340. [[CrossRef](#)]
68. Sarti, O.; El Mansouri, F.; Otal, E.; Morillo, J.; Ouassini, A.; Brigui, J.; Saidi, M. Assessing the Effect of Intensive Agriculture and Sandy Soil Properties on Groundwater Contamination by Nitrate and Potential Improvement Using Olive Pomace Biomass Slag (OPBS). *C* **2023**, *9*, 1. [[CrossRef](#)]
69. Murdiati, T.B.; McSweeney, C.S.; Campbell, R.S.F.; Stoltz, D.S. Prevention of Hydrolysable Tannin Toxicity in Goats Fed Clidemia Hirta by Calcium Hydroxide Supplementation. *J. Appl. Toxicol.* **1990**, *10*, 325–331. [[CrossRef](#)] [[PubMed](#)]
70. Fang, Y.; Wang, J.; Wang, L.; Qian, X.; Wang, X.; Liao, W.; Chen, P.; Ma, H. Densifying Hydration Products of Alite by a Bio-Inspired Admixture. *Mater. Des.* **2023**, *225*, 111490. [[CrossRef](#)]
71. Murdiati, T.B.; McSweeney, C.S.; Lowry, J.B. Complexing of Toxic Hydrolysable Tannins of Yellow-wood (*Terminalia oblongata*) and Harendong (*Clidemia hirta*) with Reactive Substances: An Approach to Preventing Toxicity. *J. Appl. Toxicol.* **1991**, *11*, 333–338. [[CrossRef](#)]
72. Allaoui, S.; Naciri Bennani, M.; Ziyat, H.; Qabaqous, O.; Tijani, N.; Ittobane, N. Kinetic Study of the Adsorption of Polyphenols from Olive Mill Wastewater onto Natural Clay: Ghassoul. *J. Chem.* **2020**, *2020*, 7293189. [[CrossRef](#)]
73. Galiatsatou, P.; Metaxas, M.; Arapoglou, D.; Kasselouri-Rigopoulou, V. Treatment of Olive Mill Waste Water with Activated Carbons from Agricultural By-Products. *Waste Manag.* **2002**, *22*, 803–812. [[CrossRef](#)] [[PubMed](#)]
74. Faschan, A.; Cartledge, F.; Tittlebaum, M. Effect of Calcium Hydroxide and PH on Organoclay Adsorption of Organic Compounds. *J. Environ. Sci. Health Part A* **1993**, *28*, 585–597. [[CrossRef](#)]
75. Stasinakis, A.S.; Elia, I.; Petalas, A.V.; Halvadakis, C.P. Removal of Total Phenols from Olive-Mill Wastewater Using an Agricultural by-Product, Olive Pomace. *J. Hazard. Mater.* **2008**, *160*, 408–413. [[CrossRef](#)] [[PubMed](#)]
76. Malkoc, E.; Nuhoglu, Y.; Dundar, M. Adsorption of Chromium (VI) on Pomace—An Olive Oil Industry Waste: Batch and Column Studies. *J. Hazard. Mater.* **2006**, *138*, 142–151. [[CrossRef](#)]
77. Langmuir, I. The Adsorption of Gases on Plane Surfaces of Glass, Mica and Platinum. *J. Am. Chem. Soc.* **1918**, *40*, 1361–1403. [[CrossRef](#)]
78. Freundlich, H. Über Die Adsorption in Lösungen. *Z. Für Phys. Chem.* **1907**, *57*, 385–470. [[CrossRef](#)]
79. Lin, J.; Zhan, Y.; Zhu, Z.; Xing, Y. Adsorption of Tannic Acid from Aqueous Solution onto Surfactant-Modified Zeolite. *J. Hazard. Mater.* **2011**, *193*, 102–111. [[CrossRef](#)]
80. Agarwal, S.; Rajoria, P.; Rani, A. Adsorption of Tannic Acid from Aqueous Solution onto Chitosan/NaOH/Fly Ash Composites: Equilibrium, Kinetics, Thermodynamics and Modeling. *J. Environ. Chem. Eng.* **2018**, *6*, 1486–1499. [[CrossRef](#)]
81. Liu, F.; Long, Q.; Gao, N.; Peng, Q.; Huo, Y.; Chen, Y.; Tang, Q.; Huang, Q.; Liu, M.; Chen, L. Effective Adsorption of Tannic Acid by Porous Dual Crosslinked Soy Protein Isolate-Alginate Hybrid Spheres from Aqueous Solution. *Chem. Eng. Res. Des.* **2023**, *189*, 250–261. [[CrossRef](#)]

82. Wei, W.; Li, J.; Han, X.; Yao, Y.; Zhao, W.; Han, R.; Li, S.; Zhang, Y.; Zheng, C. Insights into the Adsorption Mechanism of Tannic Acid by a Green Synthesized Nano-Hydroxyapatite and Its Effect on Aqueous Cu (II) Removal. *Sci. Total Environ.* **2021**, *778*, 146189. [[CrossRef](#)]
83. Zhao, Y.; Wang, L.; Zhu, L.; Gao, F.; Xu, X.; Yang, J. Removal of P-Nitrophenol from Simulated Sewage Using Steel Slag: Capability and Mechanism. *Environ. Res.* **2022**, *212*, 113450. [[CrossRef](#)] [[PubMed](#)]

Disclaimer/Publisher's Note: The statements, opinions and data contained in all publications are solely those of the individual author(s) and contributor(s) and not of MDPI and/or the editor(s). MDPI and/or the editor(s) disclaim responsibility for any injury to people or property resulting from any ideas, methods, instructions or products referred to in the content.